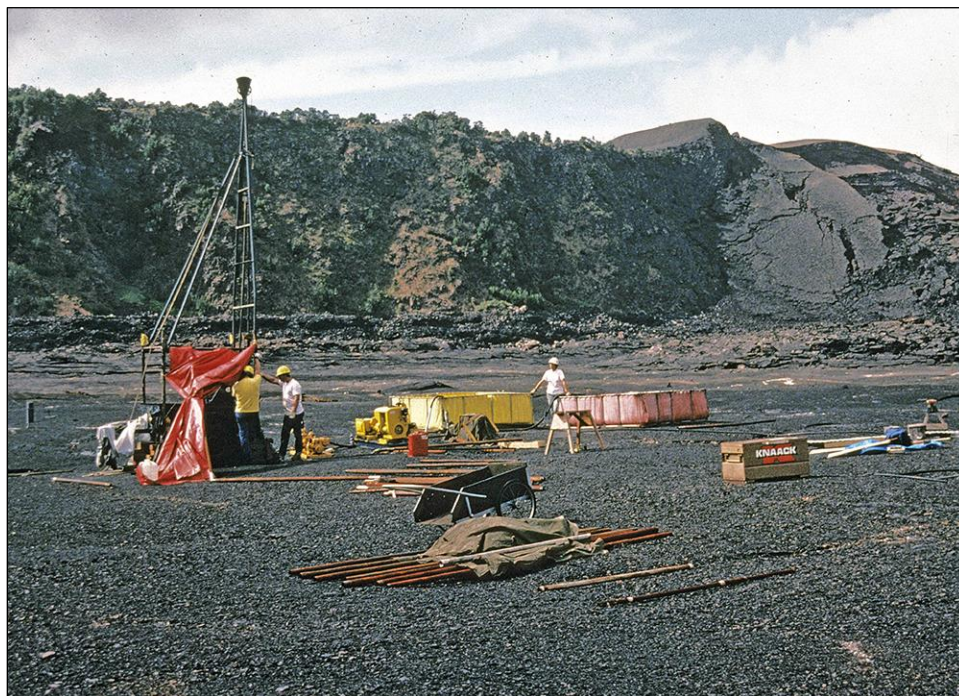![USGS logo] **USGS**
science for a changing world

Major-Element Compositional Data and Thermal Data for Drill Core from Kīlauea Iki Lava Lake, Plus Analyses of Glasses from Scoria of the 1959 Summit Eruption of Kīlauea Volcano, Hawaii

By Rosalind Tuthill Helz

U.S. Department of the Interior
U.S. Geological Survey

U.S. Department of the Interior
DAVID BERNHARDT, Secretary

U.S. Geological Survey
James F. Reilly II, Director

U.S. Geological Survey, Reston, Virginia: 2020

Cover: Drilling operation at the site of borehole KI88-2 in Kīlauea Iki lava lake. Photograph by
Jim Griggs, U.S. Geological Survey.

Contents

Figures

Tables

Conversion Factors

U.S. customary units to International System of Units

Multiply	By	To obtain
	Length	
inch (in.)	2.54	centimeter (cm)
inch (in.)	25.4	millimeter (mm)
foot (ft)	0.3048	meter (m)

International System of Units to U.S. customary units

Multiply	By	To obtain
	Length	
centimeter (cm)	0.3937	inch (in.)
millimeter (mm)	0.03937	inch (in.)
meter (m)	3.281	foot (ft)

Temperature in degrees Celsius (°C) may be converted to degrees Fahrenheit (°F) as °F = (1.8 × °C) + 32.
Temperature in degrees Fahrenheit (°F) may be converted to degrees Celsius (°C) as °C = (°F – 32) / 1.8.

Major-Element Compositional Data and Thermal Data for Drill Core from Kīlauea Iki Lava Lake, Plus Analyses of Glasses from Scoria of the 1959 Summit Eruption of Kīlauea Volcano, Hawaii

By Rosalind Tuthill Helz

Introduction

This report presents electron microprobe data on glasses and selected crystalline phases from Kīlauea Iki lava lake and glasses from the 1959 summit eruption of Kīlauea Volcano, Hawaii. Some of these data have been published previously, but the complete set has not been published before. In addition, this report includes electron microprobe data for phases in the melting experiments reported in Helz and Thornber (1987), which form the basis for using many of the glass compositions reported here to estimate quenching temperatures of the samples. Finally, because of the latter application, this report includes all useful field determinations of temperature taken in Kīlauea Iki boreholes from 1967 to 1988. These field measurements have been merged with geothermometry based on glass and Fe-Ti oxide compositions to produce a comprehensive review of all available thermal information for Kīlauea Iki. Making these datasets available completes documentation of field and chemical information on Kīlauea Iki lava lake, supplementing six previous U.S. Geological Survey (USGS) Open-File Reports listed in the References Cited.

Background and Previous Work

Kīlauea Iki lava lake was formed when much of the lava from the 1959 summit eruption ponded in Kīlauea Iki pit crater, near Kīlauea's summit (fig. 1). The eruption itself was thoroughly documented (Murata and Richter, 1966; Richter and others, 1970), and has been the object of subsequent research as well (Helz, 1987a; Helz and others, 2014a; Helz and others, 2017). Work on the lava lake also began immediately, with a leveling network installed on the lake surface by January 1960 (Pallon and others, 1994). The first drilling episode took place shortly thereafter; results from the 1960–1962 drillings were reported in Richter and Moore (1966). The lava lake was drilled subsequently in 1967, 1975, 1979, 1981, and 1988 (Helz and others, 1984; Helz and Wright, 1983; Helz, 1993). The locations of the leveling network and boreholes are shown in map view (fig. 2), and the depth of all boreholes, and hence extent of core recovery, is indicated in a cross section of the lava lake (fig. 3). Available major-element analyses of core are in Helz and others (1994) and Helz and Taggart (2010), while trace element data on samples from the 1959 eruption and the lava lake can be found in Helz (2012), Pitcher and others (2009), and Greaney and others (2017).
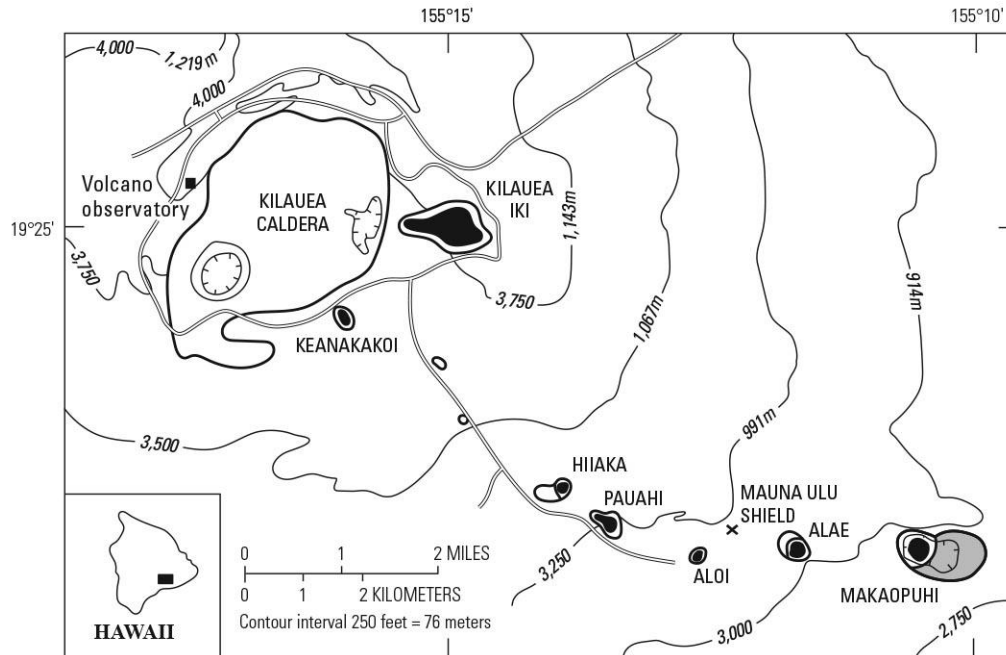
Figure 1. Index map of the summit area of Kīlauea Volcano as it appeared from 1959 to 2008. All historic lava lakes formed during that period are shown in black, with the prehistoric Makaopuhi lava lake shown by the gray stippled pattern. The historic lava lakes in Aloi, Alae, and Makaopuhi pit craters are now covered by lavas from the Mauna Ulu satellite shield, the summit of which is indicated by the "x".
Abbreviation: m, meter.
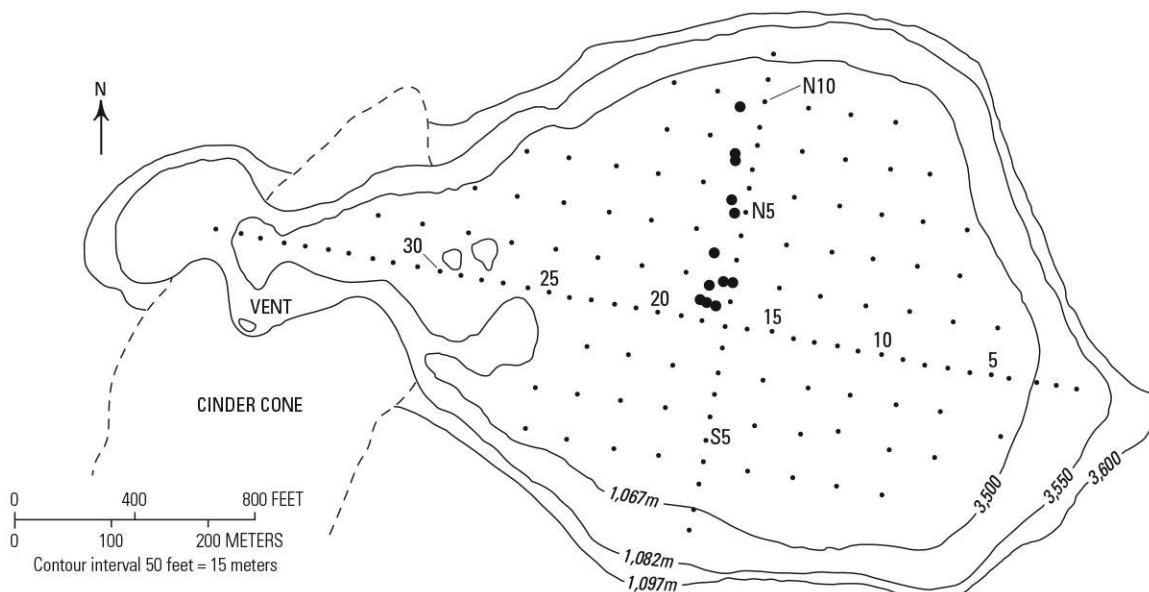
Figure 2. Plan view of the post-1959 surface of Kīlauea Iki pit crater and lava lake. The lava lake, which lies within the 3,550-foot (1,082-meter) contour, has a network of leveling stations, the locations of which are shown by the small dots. The larger dots indicate the locations of boreholes drilled from 1967 to 1988.
Abbreviation: m, meter.

2

Core obtained from the lava lake totals ~1,400 meters (m) in length, of which 210 m was partially molten when recovered, the glass having been quenched by the cooling water used during drilling. Glass data presented here include analyses from the partially molten zones of almost every core recovered, including glasses found in the 1988 cores. The report also includes glasses from the 1960–1962 cores, which were not analyzed earlier because the microprobe was not available.
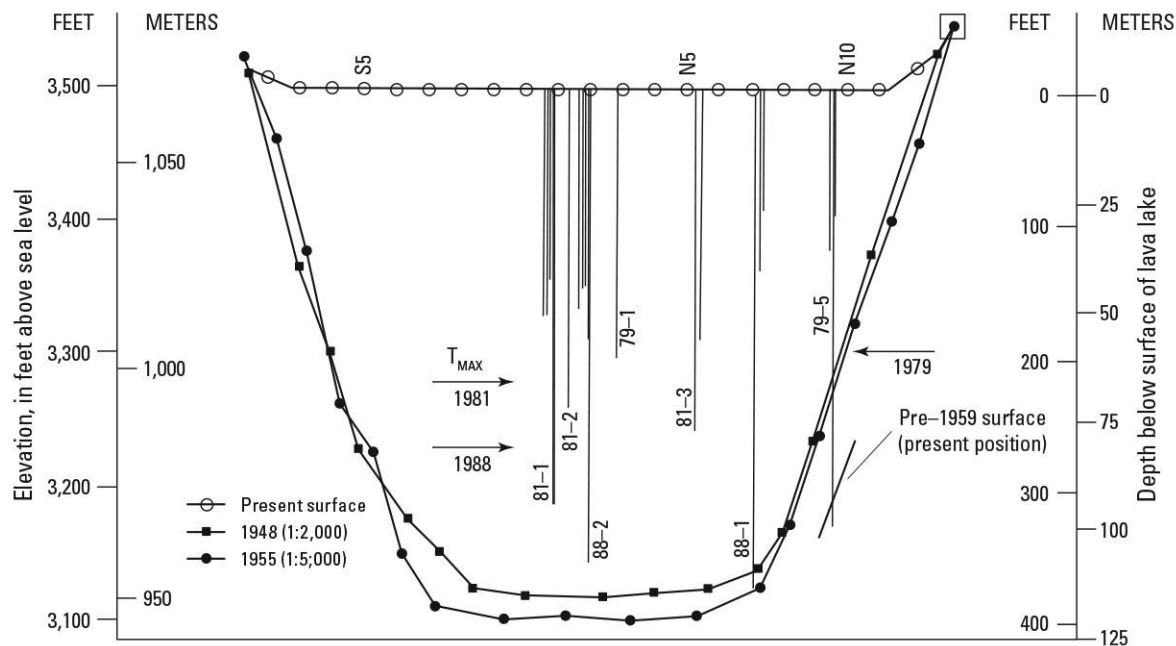
Figure 3. Cross section of Kīlauea Iki lava lake, taken along the north-to-south (from right to left) line of closely spaced leveling stations, which are labeled as shown in figure 2. The present surface of the lava lake and two pre-eruption profiles of the original pit crater prior to 1959 are shown. The pre-eruption profiles are taken from two different topographic maps: one (at 1:2,000 scale) is based on aerial photographs taken in 1948; the other (at 1:5,000 scale) is based on aerial photographs taken in 1955. Both maps were prepared by R. Jordan, U.S. Geological Survey (Flagstaff, Ariz.) The present position of the lake bottom has been intersected only at the location of borehole KI79-5. Borehole labels are shown without the KI prefix. Vertical exaggeration is approximately 4:1.

The boreholes, which mostly lie along a line 100 feet to the west of this cross section, are shown as vertical lines projected onto the section. Several of the drilling locations were occupied more than once, in order to sample the same section of the crust in several stages of development. Distances between these closely spaced holes are not shown to scale. Only the deepest hole in each cluster is labeled, for clarity. The arrows mark the position of the thermal maximum (T_{max}) in 1979, 1981, and 1988, as determined by analyzing glass in quenched, partially molten drill core using the glass geothermometer of Helz and Thornber (1987).

Electron Microprobe Analytical Techniques

Glass Analyses

Most glass analyses reported here were obtained using one of two electron microprobes at the U.S. Geological Survey (USGS), Reston, Va., available from 1979 through 2018. The first of these was an automated ARL_SEMQ nine-channel electron microprobe, with six fixed (dedicated) channels and three adjustable channels. The dedicated channels were set to Si, Al, Fe, Mg, Ca, and Mn; all other elements were on the adjustable channels. This microprobe was used for all analyses made prior to January 1993. Operating conditions were 15 kilovolts (kV), with a beam current of 0.1 microamperes. The beam diameter was 5 micrometers (μm), to reduce loss of Na_2O under the beam. The raw data were corrected online using the procedures of Bence and Albee (1968) and Albee and Ray (1970). Standards used were a basalt glass from the 1965 Makaopuhi lava lake and natural mineral standards. The original drill core sample (69-1-22; see Wright and Okamura, 1977) consisted of glass with minor amounts of plagioclase and pigeonite. Subsequently, a glass separate was made; it was evaluated as a probe standard by Jarosewich and others (1979), who referred to it as standard VG-A99 (see analyses in table 1).

Table 1. Analytical data for the Makaopuhi glass standard VG-A99 compared with the whole-rock analysis of the original drill core sample.

[Data in weight percent. Bolded numbers represent preferred values of oxides for the known-unknown glass correction procedure (see text discussion)]

Sample number	69-1-22 Whole rock	VG-A99 Glass separate
Analysis type	Gravimetric	Gravimetric
SiO_2	50.90	**50.94**
TiO_2	3.89	**4.06**
Al_2O_3	12.97	**12.49**
FeO(total)	13.20	**13.30**
MnO	**0.20**	0.15
MgO	5.18	**5.08**
CaO	9.38	**9.30**
Na_2O	2.73	2.66
K_2O	0.80	**0.82**
P_2O_5	**0.41**	0.38
Sum	99.66	99.18
Reference	Wright and Okamura (1977, table 11)	Jarosewich and others (1979, table 1)

Analyses made after January 1993 used a five-channel, fully automated JEOL JXA-8900 electron microprobe. Operating conditions were again 15 kV, with a beam current of 0.1 microamperes and with the beam diameter set at 5 µm, to reduce loss of Na_2O. The data were corrected online using a correction provided by JEOL. The standards used were the same as those used for the ARL_SEMQ analyses, except that sulfur was usually included in the list of elements analyzed.

The composition of Makaopuhi glass VG-A99 was monitored repeatedly in each glass analytical session, serving as a consistent "known unknown" throughout the entire period over which these analyses were taken (June 1979 to June 2018); occasionally basalt glass standard VG-2 and rhyolitic glass standard VG-568 (Jarosewich and others, 1979) were also checked. For each session, after all data for the unknown glasses had been corrected by the online procedures mentioned above, the resulting values of the various oxides in the unknown glasses were then adjusted for any consistent deviations between the oxide values obtained for glass VG-A99 and the reported standard analysis. These second-order corrections were made when the observed deviations were (1) large enough to affect the last significant figure in the analysis, and (2) consistent throughout the session. Maximum corrections accepted were in the range 0.95–1.05 for all oxides, with larger deviations triggering re-standardization. More typically, corrections were in the range 0.98–1.02, and were needed for only two or three oxides (of eleven in a typical analysis). The patterns of average analyses and corrections reported in Helz and others (2014b) are typical.

This second-order correction procedure was developed by Byerly and others (1977), who sought to maximize the internal consistency within a large dataset of mid-ocean ridge basalt (MORB) glasses. It was also used in Helz and Hearn (1998) to maintain consistency for glass compositions from the long-term east rift activity at Kīlauea (dates ranging from January 1983 through July 1995). Here it was used to help maintain the internal consistency of glass data from the various drilling episodes of the lava lake, with dates of analytical sessions ranging from 1979 to 1994. This was particularly important for the MgO and CaO concentrations in the glass, as these oxides (experimentally calibrated as geothermometers by Helz and Thornber, 1987) allow us to see how temperature varied in time and space as the lava lake cooled and crystallized.

For most elements, this second-order correction takes the VG-A99 values reported by Jarosewich and others (1979). However, for MnO and P_2O_5, the correction factors regularly exceeded the limits set above and re-standardization did not help. Examination of the data in table 1 for incompatible elements shows that the TiO_2 and K_2O contents are higher in the glass separate than in sample 69-1-22 (as they should be), while reported MnO and P_2O_5 are actually *lower* in the glass separate. Given that 69-1-22 contains minor amounts of plagioclase + augite, it seems unlikely that the glass would be lower in those two components. Over the years, VG-A99 microprobe analyses for MnO and P_2O_5 analyze closer to the levels observed in 69-1-22, so those numbers have been accepted as better reflecting the actual glass composition. Thus, although at first glasses were automatically referred to the Jarosewich values (as in Helz, 1987a,b), all analyses published after 1990 (including those in this report) have been referred to the higher Wright and Okamura values for MnO and P_2O_5.

All preferred values of oxides for the known-unknown glass correction procedure are highlighted in bold in table 1. The value for Na_2O has not been so marked, because the known-unknown glass mount was inevitably subject to loss of Na_2O under the probe beam, even with the beam at 5 to 10 μm in diameter. For some of the earliest analyses published (Helz, 1987a,b), Na_2O levels were adjusted to the reported VG-A99 value, but as the glass surface analyzed had less than 2.66 weight percent, the "corrected" Na_2O levels were too high. In later work, no attempt was made to apply a correction to Na_2O in the glasses.

Analyses of Crystalline Phases

Electron microprobe analyses of olivine and pyroxene from Kīlauea Iki lava lake are also reported here (appendix 1, tables 1.5–1.7 and 1.8–1.9). Like the glass analyses, these analyses were obtained at the USGS, Reston, Va. The instrument used prior to January 1993 was the ARL_SEMQ microprobe, and the JEOL microprobe was used for all subsequent analyses. Operating conditions were 15 kV with a beam current of 20 nanoamperes and a spot size of 1 to 2 μm. Counting times were 20 seconds (peak) and 10 seconds (background). Two different standard packages were used: the first, a package intended to analyze both olivine and pyroxene, included Na in the list of elements analyzed. A different package intended solely for olivine analysis omitted Na and included Ni. The compositions of the San Carlos and Marjahlati olivines were monitored to verify that analytical results for olivine were consistent from one analytical session to the next.

Analytical data on other phases are relatively sparse. This report includes some Fe-Ti oxide analyses, in particular coexisting ilmenite-magnetite pairs used to help define the variation of temperature with depth in various boreholes (see section below on temperature data). The tables reporting phase compositions from the experimental runs of Helz and Thornber (1987) include limited data on plagioclase compositions as well (appendix 1, tables 1.10–1.13). Both these data subsets were obtained using the ARL_SEMQ microprobe, and appropriate natural and synthetic phases served as standards.

In addition to this intentionally collected data, the tables having phase compositions from the experimental charges include a few analyses of crystalline phases that were "hit" in the course of seeking to determine glass composition. Because the glasses were analyzed for 8 to 11 elements, the glass standardization did allow collection of complete analyses of the various crystalline phases present. Where these data appear reasonable, they have been included, but are flagged as presumably less accurate than the rest of the datasets.

Discussion of Glass Compositional Data

Analytical Summations

Results for the analytical summations of all glasses from Kīlauea Iki lava lake and the 1959 scoria samples are presented in figures 4*A* and *B*, respectively. Three groups of glasses are distinguished:

1. Glasses from partially molten drill core in Kīlauea Iki lava lake (appendix 1, table 1.1; fig. 4*A*), for which MgO ranges from 0.02 to 6.36 weight percent and summations range from 96.47 to 100.96 percent.

2. Matrix glasses, plus the small population of analyses of low-MgO glass enclaves from the 1959 scoria (appendix 1, tables 1.2 and 1.3; fig. 4*B*), in which MgO ranges from 6.35 to 10.16 weight percent, and summations range from 98.80 to 100.89 percent. Note that there is no overlap in MgO content between the scoria glasses and those from the drill core.

3. Glasses found in embayments in olivine crystals, or interstitial to olivine in clusters of olivine crystals in the 1959 scoria (appendix 1, table 1.4; fig. 4*B*). These have MgO ranging from 6.70 to 10.00 weight percent, and summations ranging from 98.19 to 100.46 percent.

Ideally, any analytical summation would be 100 percent or very close to it, with scatter around that value generated by the uncertainties in the analytical technique. However, as can be seen in figures 4*A* and *B*, the distributions are shifted toward lower values, for two reasons. First, some components (volatiles such as H_2O, F, Cl) have never been determined, and usually S has not been determined, especially in the lava lake glasses. Second, all Fe is reported as FeO, though some of it must be Fe_2O_3, and some of the sulfur is present as SO_2. As a consequence, the peak in the summations lies between 99.0 and 100.2 percent for all three groups.

The variability in analytical summations reflects the uncertainty in the microprobe analyses, predominantly the uncertainty in SiO_2. Glasses from the lava lake (fig. 4*A*) have a wide range in summations and show more skewing toward low values. This is due mostly to systematic loss of Na_2O during the relatively long analysis routine. One consequence of the observed Na_2O loss was that no attempt was ever made to re-occupy individual glass points; thus all analyses in the analytical tables designated "R" (for replicate) are collections of new points taken on the same thin section as the original analysis. The summations are generally lowest for differentiated glasses, first because the dacitic to rhyolitic glasses contain higher alkali contents and second, because they usually occur in small pockets, where it was not possible to defocus or raster the beam. The size of this effect can be gauged by comparison between the focused-beam analyses and the occasional rastered-beam analyses (made where the size of the glass pools made rastering possible).

Summations for matrix glasses from the eruption scoria (shown in figure 4*B*) are very similar to those reported for glasses from the Kīlauea east rift eruption (Helz and Hearn, 1998). This is not surprising: the materials (degassed mafic glasses) are similar in both cases, and the analytical techniques were the same. Summations for glasses that occur interstitially in olivine clots or as embayments in olivine crystals are offset to lower values than the matrix glasses (fig. 4*B*). This is because most interstitial and embayment glasses have retained significant amounts of sulfur, with lower summations correlating roughly with higher sulfur contents. The low summations may reflect higher contents of volatiles in general, not just sulfur, but no analyses were made for F, Cl or H_2O.
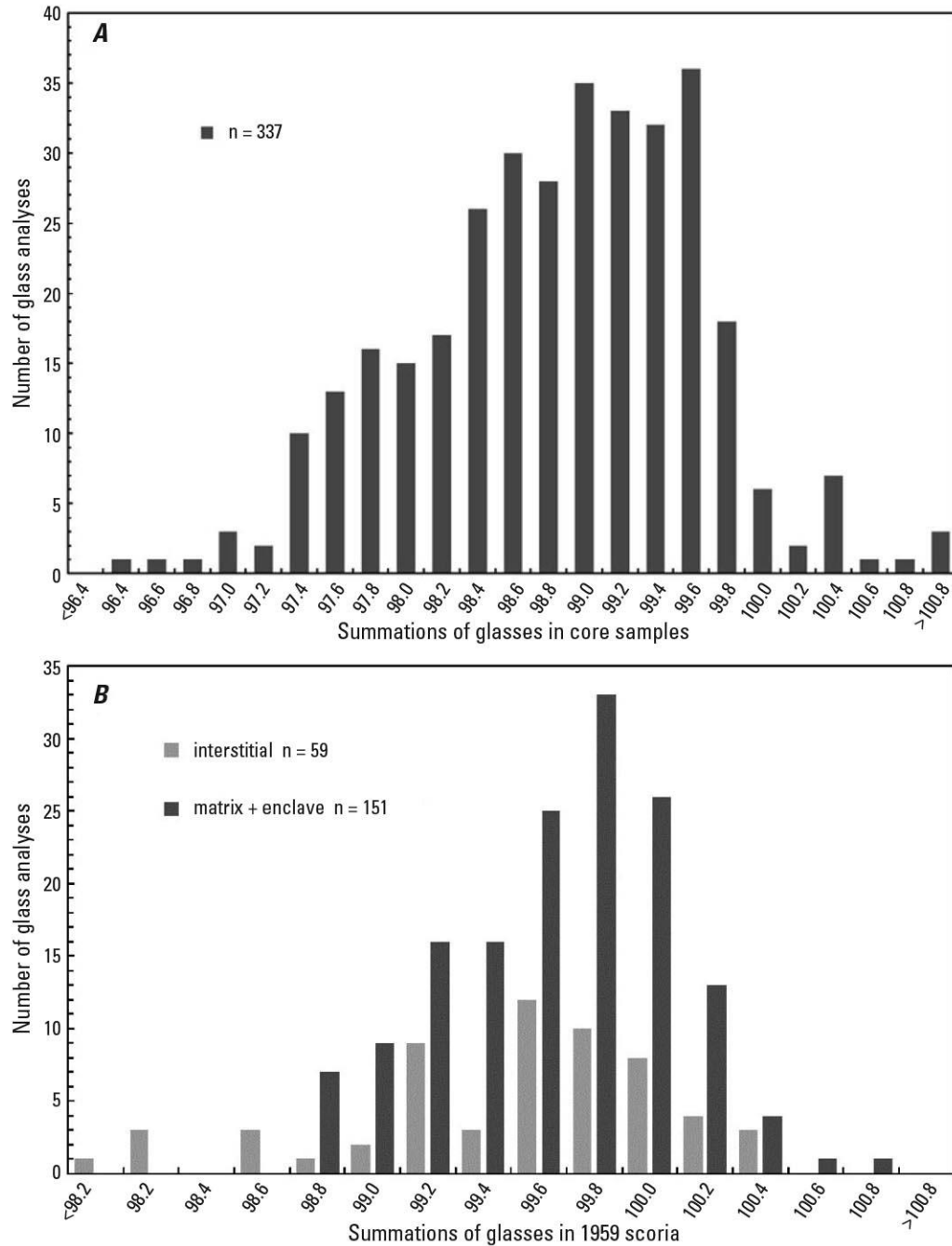
Figure 4. Histograms for analytical summations of glass analyses. *A*, analytical summations for all glasses found in the groundmass of drill core from Kīlauea Iki lava lake. *B*, analytical summations for two sets of glasses from the 1959 scoria: (1) matrix glasses and (2) glasses from interstices in olivine clots or from embayments in olivine crystals.

Glasses from Kīlauea Iki Drill Core

The first group of analyses in this report (appendix 1, table 1.1) includes 337 analyses of glasses from Kīlauea Iki drill core. Most glasses were interstitial to the multi-phase crystalline network of the drillable mush zones in the lava lake, but some were encountered at and below the crust/melt interface (see discussion in Helz and Wright, 1983). The latter (oozes, glass-in-bit samples) were almost entirely melt prior to quenching. In addition, this table includes bulk analyses of two extreme differentiates (KI79-5-163.0 and KI81-2-88.6). They were artificially fused (on a Pt-Ir strip) in order to obtain bulk compositions of these very small bodies. The analyses, the fusion process, and the quality of the results were discussed in Helz (2012, table 3); all analyses (both rastered-beam and point determinations) are presented here as well.

The bulk of the 1960–1981 glass data formed the basis for the discussion of the liquid lines of descent within the lava lake, originally presented in Helz (1987b). That paper showed first that melt compositions within each drill core varied from basaltic to ferrobasaltic, through dacitic to rhyolitic as the solidus was approached. Second, the liquid line of descent observed varied significantly from one core to another, with interstitial melts achieving higher total FeO contents during fractionation in olivine-poor regions of the lava lake. Progressively lower total FeO contents were observed as bulk olivine content increased, with differences of up to 6 percent by weight FeO at a given glass MgO content (see Helz, 1987b, fig. 4), the spread being largest between 4 and 2 weight percent MgO. This pattern was interpreted to result from re-equilibration between melt and olivine, in which olivine shifted from its original composition (average Fo_{86-87}) to more fayalitic compositions, during slow cooling of the lava lake. The patterns of olivine compositions versus depth and time in the lava lake, which are consistent with this model for the origin of the observed variations in melt composition, were reported later (Helz and others, 2014a).

The dataset presented in appendix 1, table 1.1 also includes interstitial glasses from the 1988 drill core, which were (obviously) not available in 1987. The latest data highlight another variation in the liquid line of descent in the lava lake: namely, that enrichment of P_2O_5 has varied with depth and/or time, as seen in figure 5. For all melt sequences, P_2O_5 is low at high MgO contents, increasing to the point where apatite (the only phosphate phase in the lava lake) begins to precipitate, after which it decreases to zero. For the earlier glasses (1960–1976, lying within the blue field in figure 5), P_2O_5 peaks at ~1.3 weight percent, at ~2.5 percent MgO. However, for the glasses from the 1979–1988 core, P_2O_5 levels peak at 1.6 to 1.9 percent, at ~3.0 percent MgO.

It appears that apatite crystallization requires significantly higher P_2O_5 contents in the later years, and the question is why. The most likely explanation is that the lake was slowly losing its original volatile content over time, in advance of melt crystallization. This was observable for sulfur: during all drilling episodes through 1976, abundant sulfur was released from the melt as soon as the drill string entered the partially molten zone at the base of the upper crust of the lava lake. By contrast, during the 1979 and 1981 drillings, no sulfur smell was detected (see discussion in Helz and Wright, 1983), nor was there any sulfur smell during the 1988 drilling (Helz, 1993). Could other potentially volatile species (F^-, Cl^-, or OH^-) have been lost progressively from the interstitial melt? The molten zone in Kīlauea Iki was saturated with H_2O throughout its crystallization, so OH^- should not have varied. The higher P_2O_5 concentrations required for apatite precipitation in the later part of the lake's crystallization history more likely reflect a gradual loss of F and Cl from the interstitial melts.

Another curious feature of the apatite-crystallization story is that in these same later cores, apatite precipitation becomes irregular. That is, apatite did not nucleate in every part of the matrix melt or melt pocket at exactly the same time (or to the same extent). There are five samples showing heterogeneity in CaO and P_2O_5 in glasses from a single thin section from the 1979 cores, four samples from the 1981 cores, and five from the 1988 cores. All these glasses have MgO contents at or below the peak values of P_2O_5, so they could have precipitated some apatite.
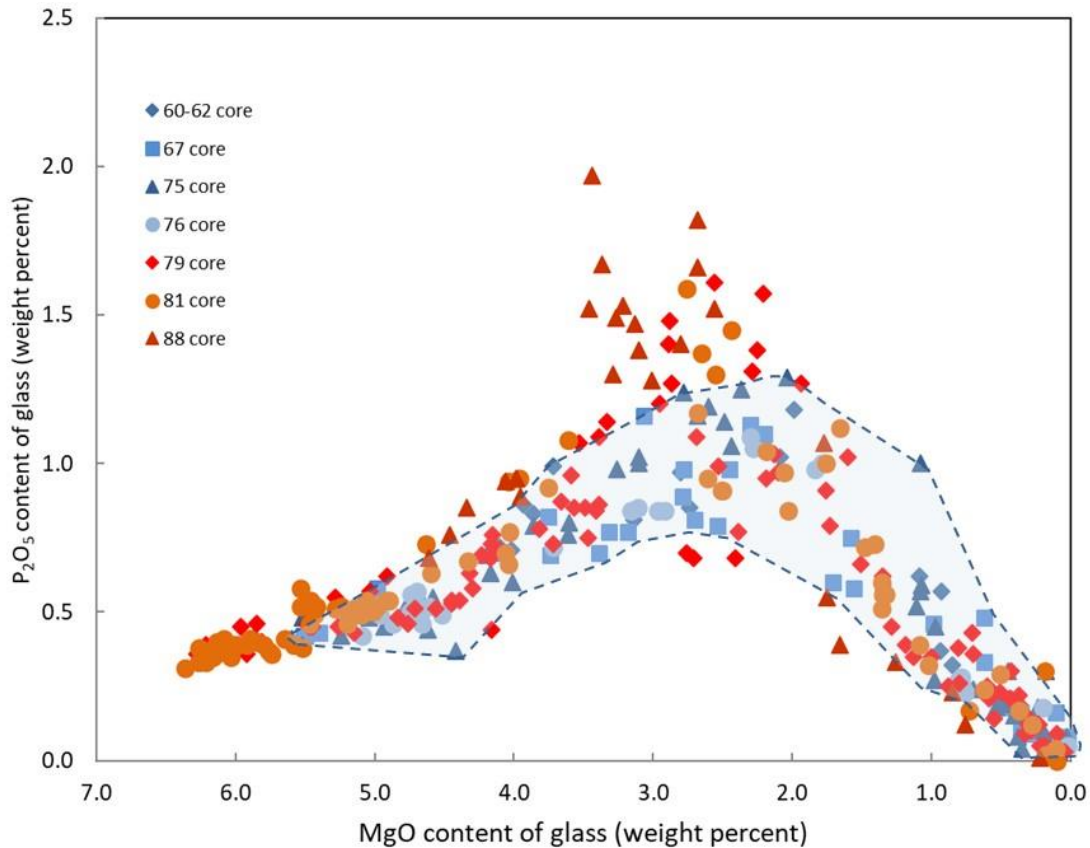
Figure 5. Graph showing P_2O_5 content of glasses from Kīlauea Iki lava lake, plotted against MgO content (both in weight percent). See text for further discussion.

Figure 6 shows P_2O_5 versus CaO in glass for these 14 samples. The figure also shows the slope of the weight ratio of P_2O_5/CaO in apatite. Most pairs (including all the matrix-to-matrix pairs) show slopes similar to the apatite line, suggesting that their compositions do indeed reflect variable precipitation of apatite, within a single thin section. Lines with other slopes suggest differential precipitation of plagioclase as well as apatite, with more plagioclase growth (= lower CaO in glass) in the matrix relative to the melt-rich veins. The most curious are two samples of 1981 core, where the matrix glasses show more extensive crystallization of both apatite and plagioclase than do the small veins in the same sections.

These glass compositions cannot all be equilibrium melts. However, it is not clear whether the divergence was caused by differential crystal growth on the quench, or by difficulty in nucleating apatite at temperature, at very low levels of F^-, Cl^-, and OH^-. Core diameter for the 1979 samples is ~3.5 centimeters (cm), while that for the 1981 and 1988 samples is ~1.5 to 2 cm, so it is curious that the pattern of inferred plagioclase precipitation (a quench effect?) is actually most conspicuous in two of the 1981 cores, not in the bulkier 1979 cores. In any case, the heterogeneity in P_2O_5 contents within single thin sections is consistent with the known low diffusion rate for P^{+5} in silicate melts.
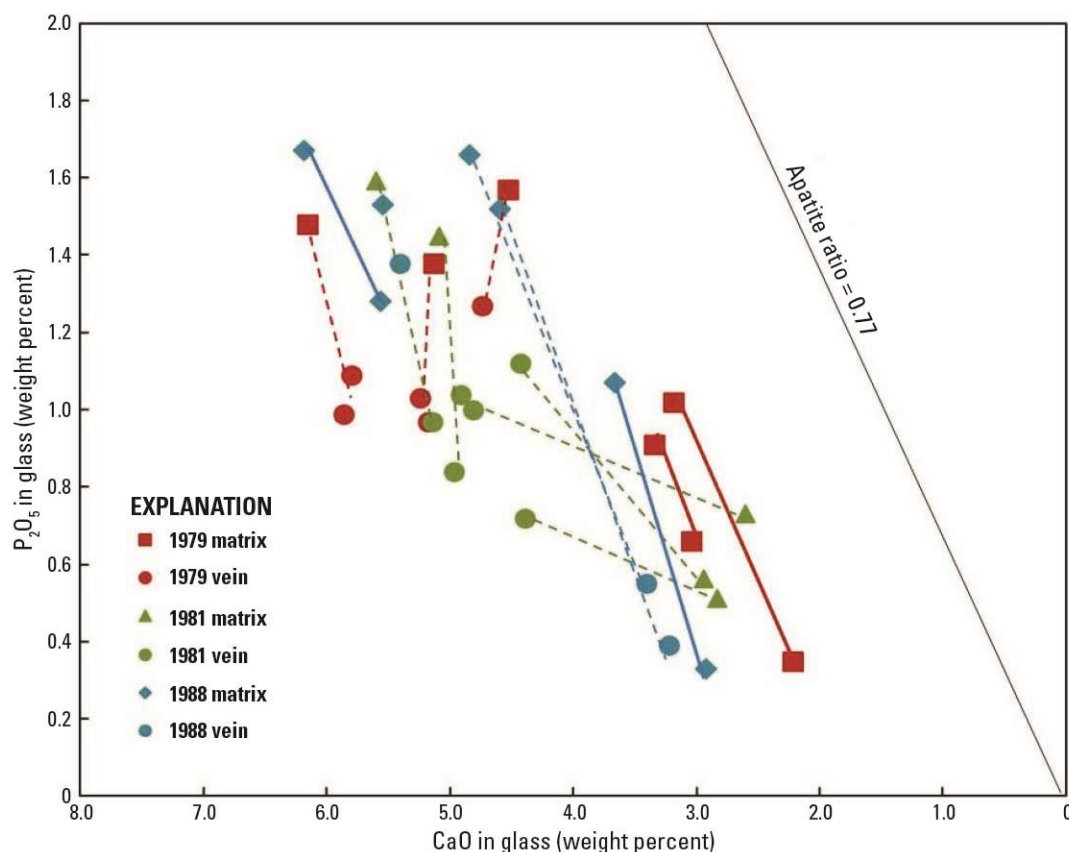
Figure 6. Graph showing P_2O_5 in glass plotted against CaO in glass (both in weight percent) for pairs of analyses from core samples where the glasses show significant heterogeneity in P_2O_5 levels within a thin section. Solid lines connect pairs of such glasses found within the olivine-rich matrix. Dashed lines connect pairs of glasses where one analysis is a melt-rich segregation ("vein") within the matrix. The slope for P_2O_5/CaO in apatite (+0.77) is shown on the right. See text for discussion.

11

Glasses from the 1959 Scoria Samples

Analytical data for glasses from the 1959 scoria samples are given in appendix 1, tables 1.2–1.4, which show matrix glasses (a), low-MgO enclave glasses (b), and interstitial and embayment glasses (c), respectively. All samples for which data are presented here were collected in real time, during the 1959 eruption, and so are the best quenched, most pristine samples available (Helz and others, 2017). Most of these glasses are in equilibrium only with olivine + chromian spinel. Even the few exceptions (glasses in early phase 1 samples and in the phase 3 scoria) have higher MgO contents than the glasses from the drill core: the minimum MgO value in table 1.2 is 6.35 percent, while the maximum in table 1.1 is 6.36 percent.

Many of these analyses have been published previously (Helz, 1987a; Helz, 2009 [electronic appendix]; Helz and others, 2017); in addition, MgO contents of many of these glasses were shown in a histogram in Helz and others (2014a). These earlier publications were selective: the analyses in Helz (1987a) were the most magnesian glasses found in each sample, while those in the Helz (2009) appendix were broad averages of as many points as were available, and the histograms excluded grand averages (so that no analysis was counted more than once in the histogram). The tables here include all analyses, variously grouped as explained in the spreadsheets.

As noted above, the range of summations for data in appendix 1, tables 1.2 and 1.3, is quite tight, although there is some skewing toward lower values, again reflecting loss of Na under the beam. Consequently, as in the lava lake glasses, replicate ("R") analyses correspond to additional points on the same thin section as the first analysis. In contrast to the lava lake glasses (of which only two were analyzed for sulfur), more than half of the matrix glasses have sulfur determinations. However, they are consistently degassed, with S ranging from 0 to 270 parts per million (ppm). Thus, sulfur degassing during the high fountaining that characterized the 1959 eruption (Richter and others, 1970) was efficient.

The small collection of analyses designated as "enclave glasses" needs a little explanation. Early on, areas of low-MgO glass were found within the higher-MgO matrix glasses in several 1959 scoria samples (Helz, 1987a). Some of these have subsequently been determined to be low in MgO because of proximity to euhedral olivine (see data in appendix 1, table 1.4); those listed in table 1.3, however, are discrete pools of clear, low-MgO glass that do not owe their character to such olivine overgrowth (quenching) effects. They do not differ in color or in other aspects of melt composition from the general matrix glass, and so are not distinguishable in thin section nor in backscattered electron images. The main indicator of their presence is that they tend to be found next to resorbed olivine, as noted in table 1.3. Figure 7 shows profiles of MgO in glass for several of these enclaves; the profiles show that the enclaves vary from tens to hundreds of micrometers in width, with MgO levels 0.5 to 1.5 percent lower than the surrounding glass.
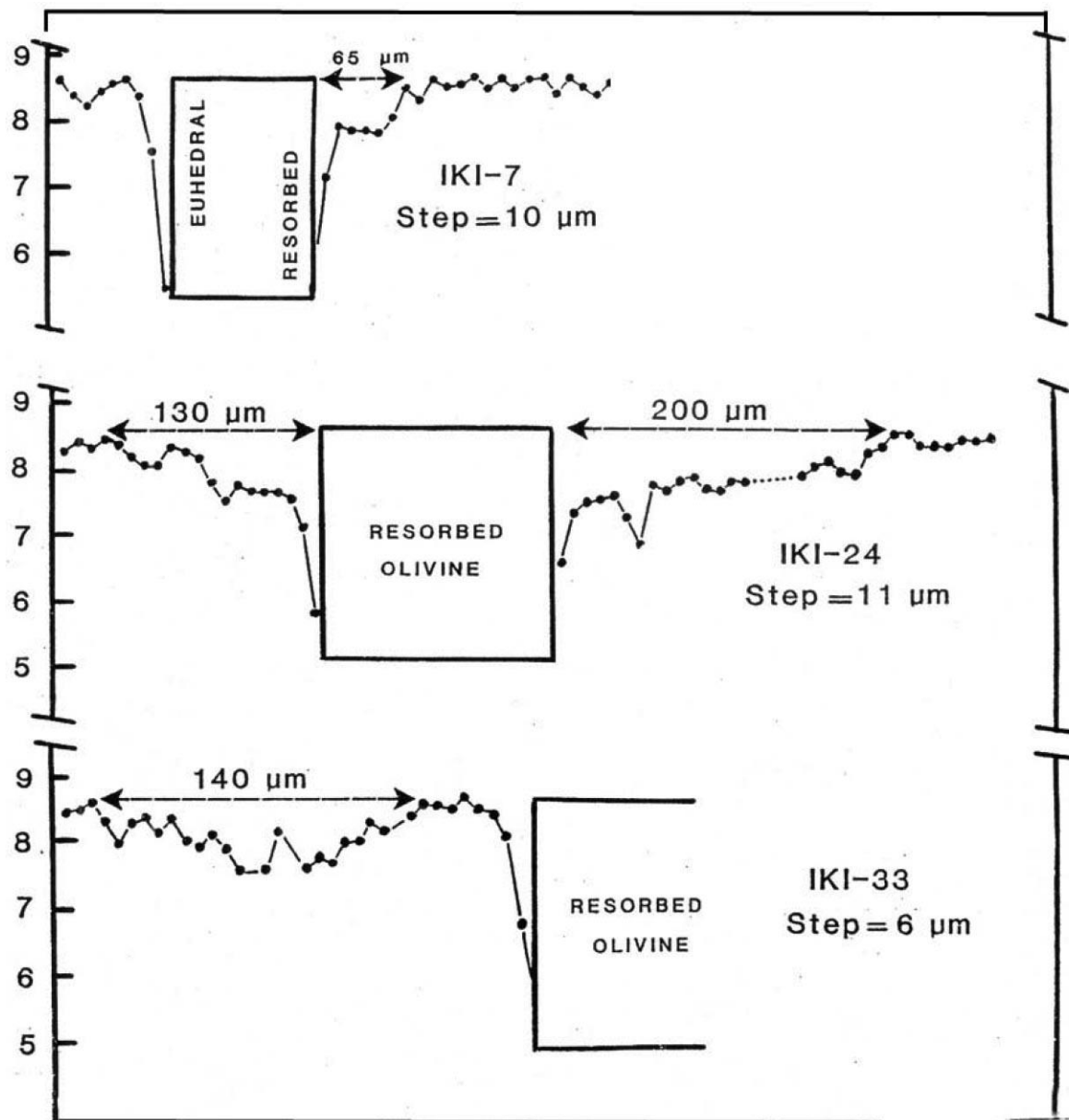
Figure 7. Profiles of MgO in glass adjacent to olivine crystals in three scoriae from the 1959 eruption. The profiles show the depth and location of low-MgO glass enclaves adjacent to olivine in Iki-7 (phase 1), Iki-24 (phase 9) and Iki-33 (phase 16). The steep drop in MgO immediately adjacent to the olivine is produced during quenching, is present at all grain boundaries, and is consistently 10 to 13 micrometers wide. The vertical position of the arrows marks the approximate MgO level of the normal matrix glass outside the enclaves.

The enclaves first appear in late phase 1 samples (see appendix 1, table 1.3; also see figure 8) but are more abundant in scoria from the later phases (7–16). They are interpreted to be small bodies of drainback that have been caught up in rising hotter melt. When surrounded by hotter melt, they would have been heated above their intrinsic liquidus temperature; thus they would resorb any grain of olivine they touched (see discussion in Helz and Wright, 1992). Figure 8 also includes MgO contents in glasses found in scoria from the 1959 ejecta blanket;

13

these have been plotted at their inferred eruptive phases, as reported by Stovall and others (2012) and Rae and others (2016). The MgO contents of these glasses partly overlap the enclave glasses but most are significantly lower than the dominant matrix glasses in the real-time scoria samples. It is possible that the small areas with microlite development noted by Stovall and others (2012) in samples from phases 15 and 16 (and interpreted by them as drainback) are partially devitrified equivalents of these glass enclaves; the MgO data in figure 8 suggest that the ejecta samples have undergone some post-eruptive cooling and crystallization. However, none of the enclaves in table 1.3 contains microlites or other signs of devitrification. In fact, the entire collection of analyses of scoria glasses presented here were taken on clear, microlite-free glass within each sample.
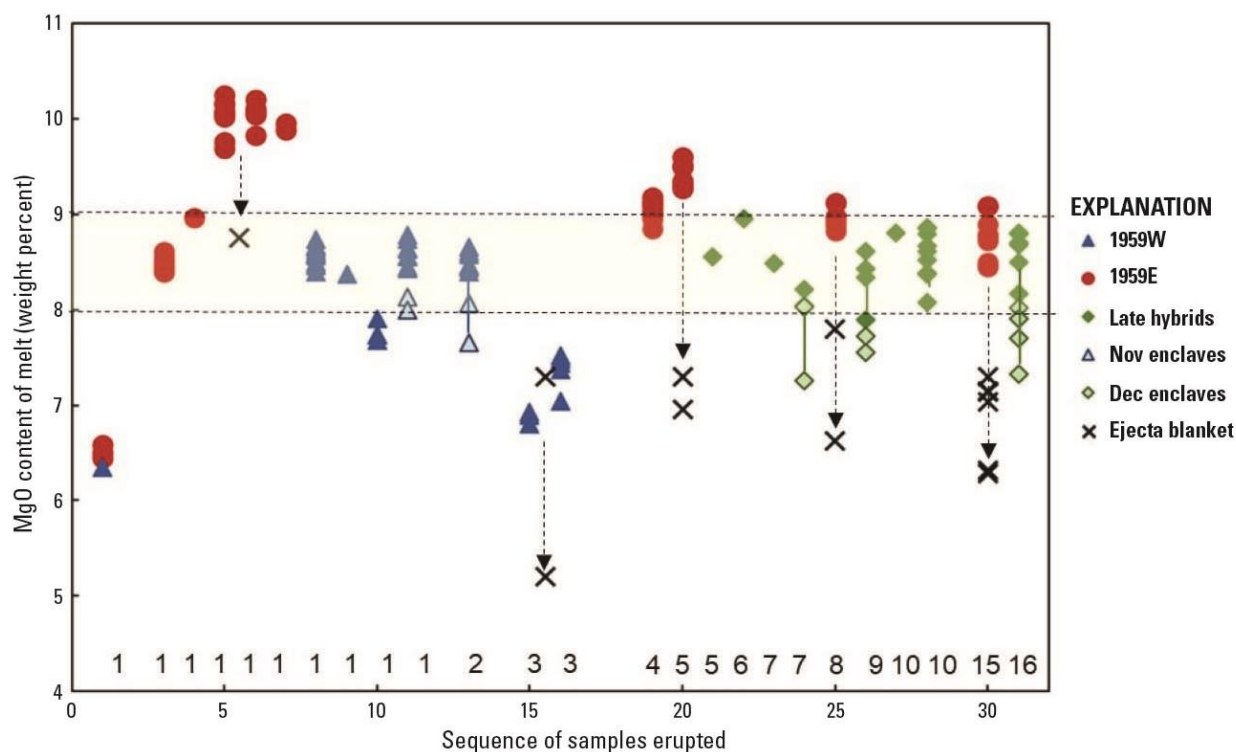
Figure 8.   Graph showing MgO content in glasses from the 1959 eruption scoria, plotted in the sequence they were erupted, with the eruptive phases indicated above the abscissa. Solid symbols are matrix glasses from appendix 1, table 1.2; open symbols are enclave glasses from appendix 1, table 1.3. The x symbol marks the MgO content of glasses from the 1959 ejecta blanket as reported in Stovall and others (2012) and Rae and others (2016). The field between the horizontal dashed lines encompasses the bulk of the matrix glasses from scoria samples collected in real time during the eruption. See text for discussion.

The final set of data from the 1959 scoria samples is a collection of analyses found either in embayments in olivine, or as interstitial melt within clusters of olivine crystals. Unlike the matrix and enclave glasses, which are mostly averages of multiple points, the table 1.4 (appendix 1) analyses are almost entirely for single points: this is because their sulfur content varies so strongly from one point to the next. It is highest in the interior of the embayment or interstitial area, decreasing systematically toward the mouth of the embayment or the margin of the olivine clot. These gradients document the degassing history of individual olivine clusters in the scoria and have been found to correlate with changes in the redox state of the glass (Helz and others, 2017).

14

Discussion of Analyses of Crystalline Phases

Olivine Compositions from Kīlauea Iki Lava Lake

Kīlauea Iki lava lake contains abundant olivine, so that the results presented here necessarily represent only a fraction of the crystals available. For each sample analyzed, the analysis routine included (1) collecting data on olivine phenocrysts, from core out to rim, always including the largest crystal in the thin section, and (2) collecting data on microphenocrysts and groundmass olivine. Thus, points a4, a5, a6, and a7 for sample KI67-3-75 (appendix 1, table 1.6) are a traverse on one of the largest olivine grains in that sample.

The "in situ" olivine dataset (appendix 1, table 1.5) includes analyses of all small olivine and rims on olivine phenocrysts, that is, any olivine that could possibly have grown post-eruptively in the lava lake. These data are presented as averages, with the range of compositions indicated (as in table 4 in Helz and others, 2014a). The second category comprises phenocryst cores, which definitely existed in the magma prior to the eruption; for these, individual point analyses, including their rim compositions, are shown in appendix 1, table 1.6. Note that the rim compositions in table 1.6 are included in the averages and ranges shown in table 1.5. In addition, limited data on olivine from dunite clusters described in Helz (1987a) are shown in table 1.6, and a third table (table 1.7) includes traverses on four olivine megacrysts found in the lava lake.

The data show a consistent pattern of olivine re-equilibrating with melt over time, with the extent of re-equilibration being controlled by (1) the size of the crystal, (2) local bulk composition (olivine content), (3) the rate of cooling experienced by the sample, and (4) the total length of time in the lake prior to sampling, as discussed in detail in Helz and others (2014a). The most slowly cooled parts of the lake show extensive re-equilibration of olivine from original compositions (averaging Fo_{86-87}) to Fo_{80-81}. In some samples, even phenocryst cores have reached these compositions (see data in table 4, also figures 18a and 18b, all in Helz and others, 2014a), though this process is not uniform: Scowen and others (1991) report a few surviving high-Fo cores in samples where none were found in this study (appendix 1, table 1.6).

The 1959 scoria (and hence the lava lake) contain rare olivine megacrysts, which are very large (1–2 cm in dimension) skeletal crystals. Three were shown in figure 20 in Helz and others (2014a). Since then a fourth such crystal has been found, representing even more extensive compositional re-equilibration than the others (fig. 9, this report). During progressive re-equilibration of olivine in Kīlauea Iki, these large crystals retained their original high-Fo compositions somewhat longer than the normal phenocrysts (see, for example, megacryst KI81-1-238). However, the two recovered in the 1988 core, especially the deepest crystal that cooled the slowest (KI88-1-255), have the same compositional range as the in-situ olivine. This same pattern can be observed in the limited data for dunite clots included in appendix 1, table 1.5; these bodies (discussed in Helz, 1987a) are similar in size to the megacrysts.

The fourth megacryst was part of a small number of olivines for which ZnO determinations were made, and the results are included in appendix 1, table 1.7. Limited data on ZnO in olivine for four other samples are shown in table 1.6; these results were presented in table 4 of Helz (2012), and their significance discussed in that report.
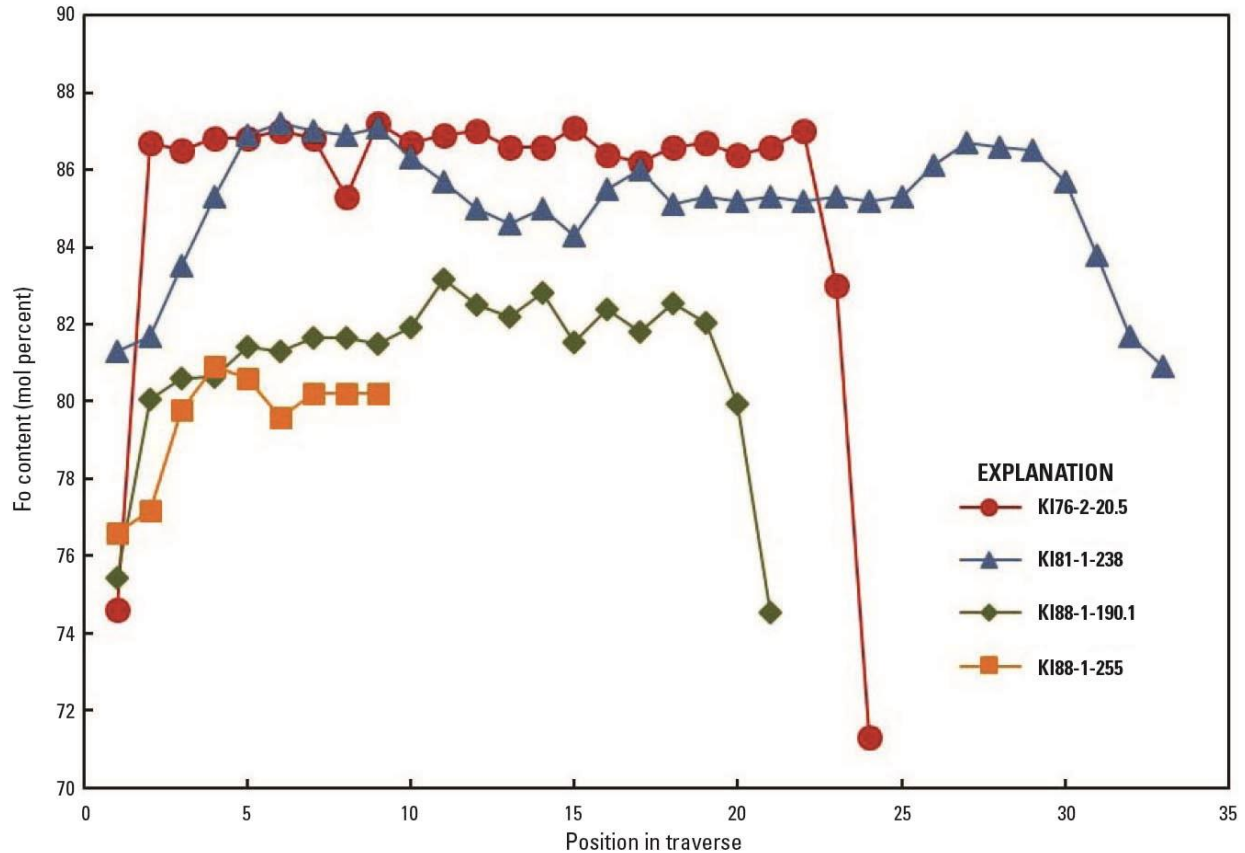
Figure 9. Graph showing variation of forsterite (Fo) in four olivine megacrysts from Kīlauea Iki lava lake. This figure differs from figure 20 in Helz and others (2014a) in that the abscissa here is the position of the various points in the traverses, not distance. This is because for two of the traverses shown here (KI88-1-190.1 and KI88-1-255), it was necessary to modify step locations by hand to avoid the numerous voids in these skeletal crystals. The step size in all cases is ~0.5 millimeter.

Local Effects on Olivine Compositions

As discussed above, the vast bulk of olivine in Kīlauea Iki has consistently re-equilibrated to more Fe-rich compositions, subject to variations in the size of the crystal or aggregate and to the details of the cooling history of the samples. This re-equilibration produced significant variations in the local liquid line of descent, and in the mineral assemblages for phases that crystallized subsequent to this re-equilibration, as originally laid out in Helz (1987b).

Two other, more local effects have been observed. They are (1) oxidation of olivines by trapped air in foundered crust and (2) anomalous cooling and zoning developed in core from boreholes close to earlier holes, especially notable in later cores from the 1981 drilling.

Foundered crust is widespread in Kīlauea Iki lava lake as summarized in Helz (1993). In most places, air escaped relatively completely from the highly vesicular layers within the foundering crust. However, in the deepest part of the wedge of foundered crust cored in hole KI67-1, from ~60 to 72 feet (ft) (18–22 m) (Helz and others, 1984), the olivine is extensively oxidized, with precipitation of fine-grained magnetite at the margins and within the olivine grains. The appearance of this "blackened olivine" core and the resulting extremely forsteritic olivine composition ($Fo_{91.8}$) are shown in figure 10 and table 2. Less extensive development of

16

oxide precipitation has been observed in other blocks of foundered crust and may have shifted the olivine compositions there as well.

In most drilling efforts, the holes were few and widely spaced, so each recovered core was not affected by prior drilling of adjacent holes. Exceptions include core from hole KI79-3, which was drilled a few weeks after the re-entry of hole KI75-1 (designated KI75-1R in Helz and others, 1984), which was 13 to 16 ft (4–5 m) away. The other was hole KI81-5 (drilled several weeks after KI81-1 and immediately after KI81-7, both 10 to 20 ft (3–6 m) away; see Helz and Wright, 1983). There are no obvious anomalies in the olivine zoning in core from KI79-3 (see appendix 1, table 1.6; also see discussion in Helz and others, 2014a). However, two studies of olivine from the hottest and most olivine-rich section of KI81-5 (sample KI81-5-254.5, used by Teng and others, 2011; Sio and others, 2013) found olivine with significant Fo zoning (out to Fo_{70-72}), as well as zoning in Mg and Fe isotopes. Olivine from this depth range (205–270 ft, or 62–82 m) in the first hole drilled (KI81-1) shows Fo content varying between 81.7 and 79.3; there is no discernable zoning in backscattered electron imagery (fig. 19 in Helz and others, 2014a). The sharp, narrow marginal zoning seen in KI81-5 samples must reflect the influence of the prior drilling of two holes, plus the engineering studies done in KI81-1 (Hardee and others, 1981; Helz and Wright, 1983). Thermal effects over this distance, observed during downhole thermocouple measurements, are discussed below.
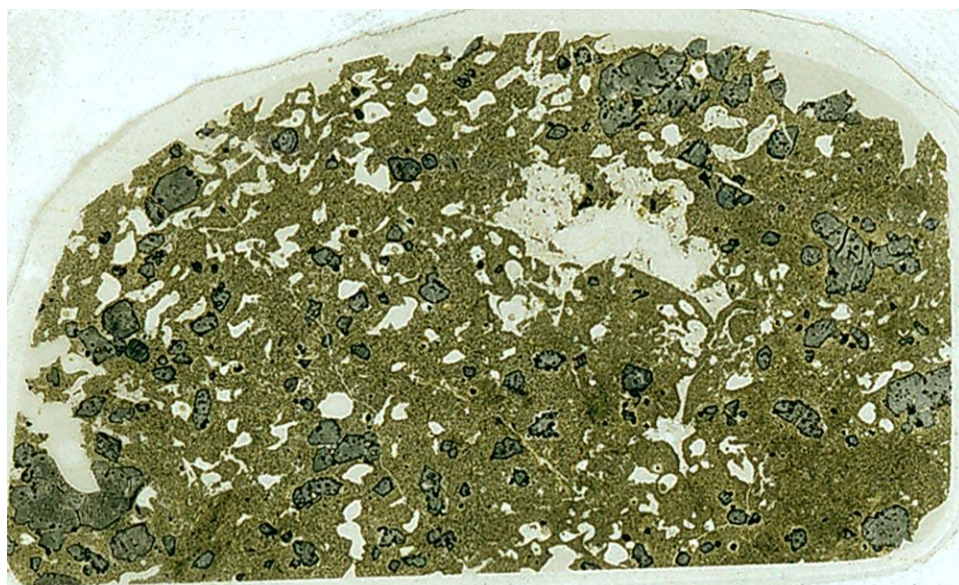
Figure 10. Photomicrograph of the entire thin section of sample KI67-1-69.5 (field of view is 2 centimeters across). All olivine phenocrysts (greenish crystals with black rims) in this sample of foundered crust have been oxidized by interaction with air trapped in the vesicles when the crust sank in the lava lake. The vesicles (white areas within groundmass) are mostly deformed; the largest contains a pool of rhyolitic melt that has partly filled the vesicle.

Table 2. Olivine and orthopyroxene analyses from oxidized foundered crust sample KI67-1-69.5.

[Data in weight percent]

	Olivine	Orthopyroxene
No. points	6	1
SiO_2	40.58	56.32
TiO_2	0.03	0.06
Al_2O_3	0.03	0.58
Cr_2O_3	0.01	0.25
FeO	8.00	6.16
MnO	0.35	0.29
MgO	50.01	34.07
CaO	0.10	1.04
NiO	0.27	0.07
Sum	99.38	98.84
Mg/(Mg+Fe)	0.918	0.908

Pyroxene Relations and Compositions in Kīlauea Iki Lava Lake

Though olivine compositions in Kīlauea Iki have been documented extensively, as reviewed above, the available data on pyroxenes is comparatively limited. All core samples from the lava lake were recovered at temperatures ≤1,142 °C, so they contain augite and plagioclase, in addition to the olivine and chromian spinel found in the eruption scoria. In addition to the ubiquitous augite, pigeonite and/or orthopyroxene also occur in the lower temperature core samples. Pigeonite begins to crystallize at ~1,084 °C, and orthopyroxene at ~1,087 °C (see appendix 1, table 1.8). This is well below the temperature of first appearance of the Fe-Ti oxides, which lies between 1,105 °C and 1,102 °C, as indicated by the location of peak TiO_2 in table 1.1 (see also Helz, 1987b; Helz and Thornber, 1987).

The occurrence of pigeonite versus orthopyroxene (like magnetite + ilmenite versus ilmenite ± ferropseudobrookite) is controlled by a combination of melt composition and local bulk composition. Relatively olivine-poor intervals (with relatively Fe-rich interstitial melts) contain pigeonite (and magnetite + ilmenite). The olivine-rich core samples (from 1981 and 1988) have Fe-depleted interstitial melts, which crystallize orthopyroxene and ilmenite ± ferropseudobrookite, as detailed in Helz (1987b). Table 1.8 in appendix 1 includes all pyroxene compositions obtained for olivine-phyric matrix rock, as cross referenced in table 1.6. Table 1.9 contains limited data for pyroxene from internal differentiates in drill core KI79-3 and KI79-5, including two segregation veins (samples KI79-3-158, KI79-3-172.9) and two small extreme differentiates (samples KI79-3-157.7, KI79-5-163.0).

18

Note that contrary to the discussion in Murata and Richter (1966), there is no early, coarse, phenocrystic augite in Kīlauea Iki. However, a single oikocryst of augite (in sample KI75-1-134.4; see figure 11) has been found and its composition is given in appendix 1, table 1.8. Augite otherwise occurs as small, equant crystals in the groundmass of the olivine-phyric matrix rock. Its composition is quite variable within a single sample, suggesting that augite composition does not re-equilibrate as crystallization proceeds on the time scale of cooling of the lava lake. Augite is the principal reservoir for Cr_2O_3 apart from chromian spinel, the latter being present in the drill core almost exclusively as inclusions in olivine. The affinity of augite for Cr_2O_3 is strong enough that spinel not enclosed in olivine is completely eliminated by ~1,140 °C. As table 1.8 shows, there is an inverse relationship between Cr_2O_3 and FeO in augite, consistent with the idea that the earlier augite takes up Cr_2O_3 preferentially.

The appearance of pigeonite, always a groundmass phase, is similar to that of augite. Orthopyroxene, however, occurs both as groundmass crystals and as oikocrysts. The oikocrysts are common, often approaching the smaller olivine phenocrysts in size (see figure 21 in Helz and others, 2014a). The most noticeable feature of the orthopyroxene oikocrysts is that the only phases that survive inside them are plagioclase and Fe-Ti oxide: the groundmass olivine and augite are consumed during growth of the oikocryst. Compositionally, the orthopyroxene is a late groundmass phase, relatively Fe-rich with very low Al_2O_3 content. It is similar to orthopyroxene from differentiated lavas from the 1955 and 1960 eruptions of Kīlauea (Anderson and Wright, 1972; Helz and Wright, 1992).
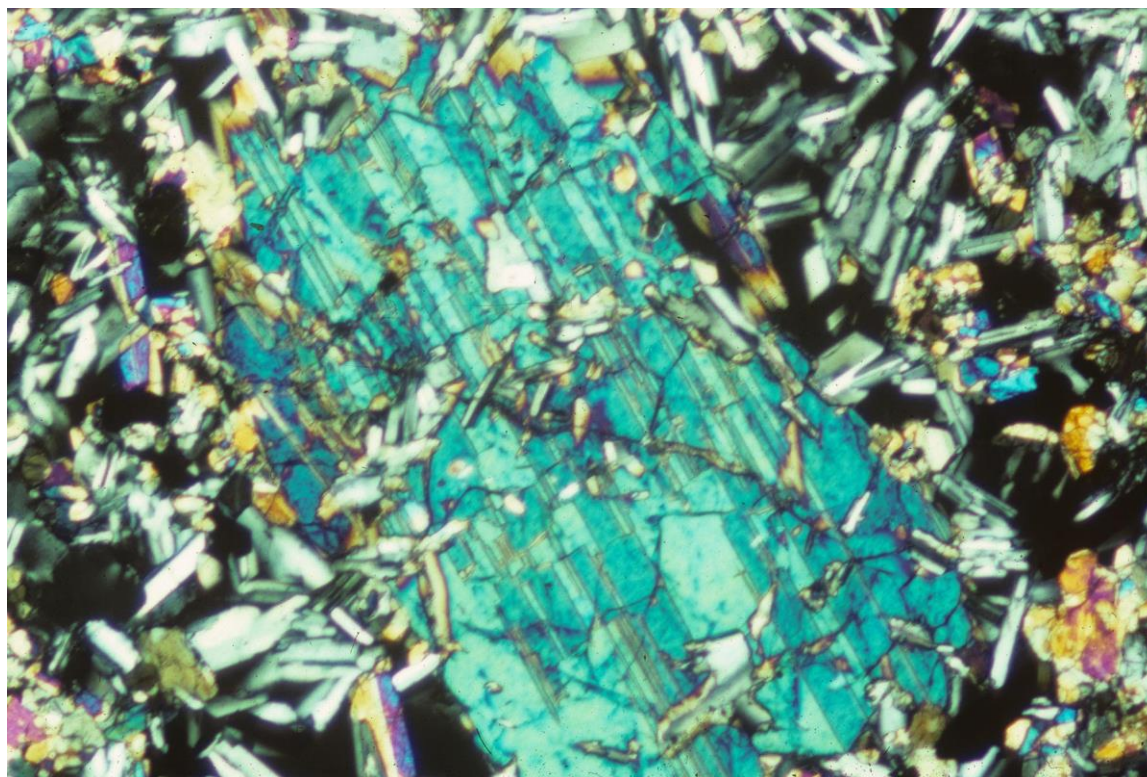
Figure 11. Photomicrograph of an augite oikocryst in sample KI75-1-134.4 (field of view is 2 millimeters across; nicols crossed). The included plagioclase shows that this is not a phenocryst. The composition of this grain is given in appendix 1, table 1.8.

The final data from the lava lake are from two extreme differentiates that formed when melt migrated into open fractures. The first of these was a near-rhyolitic glass coating an open fracture between two segregation veins (fig. 12). As the columnar joints do not ordinarily extend into the partially molten zone (Helz, 1993), this fracture is inferred to have formed during drilling of nearby hole KI75-1R three weeks earlier (Helz and others, 1984). The source of that part of the coating (sample KI79-3-157.7) was the underlying segregation vein (sample KI79-3-158; see figure 12). The glasses from these two samples are in appendix 1, table 1.1, and the pyroxene data are in tables 1.8 (pyroxenes in the wall rock) and 1.9 (pyroxenes in the coating and in the segregation vein).

Rippled surface of glass coating on new columnar joint fracture

Figure 12. Photograph of a section of core KI79-3, showing a vertical glass-coated surface that opened up between two segregation veins during the 1979 drilling. The upper vein (which extends from 156.9 to 157.0 feet [ft]) is to the left, and the lower vein (which occurs at 157.9–158.2 ft) is to the right. There is an area of bare rock between the rippled glass films that have crept in from the two segregation veins. The glass and pyroxene analyses described as KI79-3-157.7 in appendix 1, tables 1.5 and 1.8, are from the lower (right) coating. The glass and pyroxene analyses from KI79-3-158 are from the lower (right) segregation vein. See text for further discussion. Scale is in inches.

The second extreme differentiate (KI79-5-163.0) was also produced when melt migrated into and partly filled an open fracture. This small body has been analyzed for trace elements (Helz, 2012), and its glass and bulk compositions (appendix 1, table 1.1) and pyroxene compositions (tables 1.8 and 1.9) are presented here. The source wall rock was subsolidus when collected, so it contains no glass; the glass in the vein is inferred to be metastable.

Comparing the pyroxene compositions for these late differentiates with those in their immediate source or host shows that bulk compositional control on phase composition is very local: the pyroxenes found within the small differentiates are more Fe-rich than those in the source or in the adjacent wall rock. This is true even for the 157.7/158 pair where the glass composition is the same in the coating, the wall rock, and the segregation vein (appendix 1, table 1.1). The data in table 1.9 also define the limits of compositional variation for pyroxenes in Kīlauea Iki lava lake.

Discussion of Analyses from Melting Experiments

The final set of analytical tables in this report presents data on the melting experiments initially described in Helz and Thornber (1987). The experiments were conducted at 1 atmosphere (atm), using mixtures of H_2 and CO_2 to constrain the oxygen fugacity of the samples to ~nickel-nickel oxide (NNO) conditions. Water is formed as the gas mixture reacts, so the experimental melts contained some water; infrared spectral analysis of glasses in two near-liquidus experimental runs (KI75-1-143.8, run no. 18; and KI67-3-83.8, run no. 1) found 157 ppm and 169 ppm, respectively (P. Wallace, University of Chicago, written commun., 1993). These levels are an order of magnitude lower than those determined for natural glasses from the lava lake (table A on p. 25 in Helz and others, 1994), but the latter glasses were quenched at pressures between 3 and 6 atm, not at 1 atm.

Helz and Thornber (1987) found that the MgO and CaO contents of glasses in the lava lake varied linearly with temperature, for glasses in equilibrium with olivine (for MgO) or with the assemblage olivine + augite + plagioclase (for CaO). Accordingly, the concentrations of those components in the glasses have been used to assign quenching temperatures to all glassy core samples from the lava lake. The geothermometry results will be discussed below, in the sections reviewing all data relevant to the cooling history of the lava lake.

Data presented here include the glasses that formed the basis of the calibration (appendix 1, table 1.10), which were also published in an electronic appendix to Helz (2009). In addition, this report includes analyses for olivine (table 1.11), pyroxenes (table 1.12), and plagioclase (table 1.13). Table 1.10 also includes the bulk compositions of the two starting materials, but with all iron as FeO (original analyses are in Helz and others, 1994), to facilitate comparison with the glass compositions found in the near-liquidus runs.

The phase assemblages in the starting materials (KI75-1-143.8 and KI67-3-83.8) were characterized as part of the experimental project; most of those data were presented above, in appendix 1, table 1.1 (glasses), tables 1.5 and 1.6 (olivines), and table 1.8 (pyroxenes). Data for plagioclase in the starting materials has been included in table 1.13, for comparison with plagioclase compositions found in the melting experiments. Comparing mineral compositions found in the experiments with those originally present in the starting material suggests that the runs, for the most part, contain little relict material. The one exception is an olivine core present in run no. 7 (starting material KI75-1-143.8, table 1.11), which still has one Fe-rich core characteristic of re-equilibrated olivines from that level in the lava lake.

Notes on the Analytical Tables (Appendix 1)

All data for glasses, mafic (olivine + pyroxene) phases, and the experimental charges are contained in appendix 1 as Excel spreadsheet tables, which are available for downloading at https://doi.org/10.3133/ofr20201012. Most of the columns in the tables are self-explanatory. This section provides additional information on sample labeling conventions, and on the detailed descriptions of glass areas or crystals analyzed, as follows:

1. **Sample numbers:** For samples from Kīlauea Iki drill core recovered between 1967 and 1988 (tables 1.1, 1.5–1.7, and 1.8–1.9), the first column shows the drill core sample number (for example, KI67-3-70.0), which indicates in this instance that the sample is from the third hole drilled in 1967, at a depth of 70.0 ft. In table 1.1, samples from the early (1960–1962) cores are numbered as in Richter and Moore (1966). In these tables, numbers marked "R" indicate that the analysis is a second set of points taken on the glass (or olivine) on the same thin section at a later date. In no instance were individual points relocated and reanalyzed. Tables 1.2–1.4 present glasses from the 1959 eruption scoria, which are designated by their original field numbers. Where data come from different thin sections, individual sections are given additional numbers; for the mounts used in the X-ray absorption near-edge structure (XANES) study (Helz and others, 2017), the number includes an "X". Where more than one crystal or clusters of crystals within a section have been investigated, there is an additional number designation in the sample number in the first column (column A). Uniquely in table 1.6 (olivine phenocryst cores), the sample number in column A may have a letter designation (for example, KI67-3-75-a4). This indicates which of the individual point analyses in that table are from a particular olivine crystal: a different letter indicates points on a different olivine crystal.

2. **Sample descriptions:** For table 1.1, column B provides a description of the sample and/or type of glass analyzed. Thus, "matrix glass" is glass within the olivine-phyric matrix, while "segregation" or "vein" indicates glass from within a segregation or other internal differentiate. In tables 1.2–1.4, the phase of the eruption and the eruption date of the sample are in columns B and C, respectively, with additional information on either the location or distinctive character of the glass analyzed in column D. In the other tables (1.5–1.7 and 1.8–1.9), such supplemental information is in the "Comments" column.

3. **Microprobe analyses:** The next two columns in tables 1.1–1.5 and 1.8–1.9 contain the date of the microprobe session and the number of points included in the analysis. In tables 1.6 and 1.7, the date of the microprobe session is given, and each analysis represents a single point. In table 1.7 (traverses on megacrysts), the following column contains the step number in the traverse. The oxide data in the following columns are all in weight percent, with all Fe reported as FeO, followed by the analytical summation. Where an element was not analyzed, this omission is indicated by "nd" for "not determined." Analyses of sulfur (S in ppm) in the 1959 glasses (tables 1.2–1.4) are shown in a separate column, as most of the sulfur is sulfide, not sulfate (Helz and others, 2017).

4. **Temperature information:** In table 1.1, both T_{MgO} and T_{CaO} values are given for most glasses, based on the Helz and Thornber (1987) calibration. T_{MgO} has not been assigned for rhyolitic glasses in olivine-free samples (per Helz and Thornber, 1987). For a few rastered-beam analyses plus those on fused glass samples ("BULK" in sample description), no temperatures have been assigned, as the bulk composition obtained may not equal an actual melt composition. Values in italics indicate that the glass is considered to be metastable (see discussion below). The T_{MgO} and T_{CaO} values relevant to a particular sample are also given in tables 1.5–1.7 and 1.8–1.9, where appropriate.

Finally, users of this report should note that all depth measurements herein are in feet and tenths of feet (not feet and inches, nor meters). This is because the drilling equipment that was used imposed that system on both the depth of the boreholes and the depths of recovery of all drill cores. The core boxes are labeled in decimal feet, as are the drillers' blocks. These notations and blocks have been retained for the core in storage at the Smithsonian National Museum of Natural History, to facilitate navigation in sampling the core. Consequently, the depths for all individual samples (for example, KI67-3-70.0) in all tables and figures are consistent with the field process and subsequent labeling. This convention has also been followed in the sections below, as the depths for all the thermocouple profiles made were in feet and tenths of feet. Again, this usage is consistent with the available field records.

Thermal Data on Kīlauea Iki Lava Lake—Methods

The investigation of Kīlauea Iki has included many attempts to obtain temperature data, to assess the cooling behavior of the magma body over time. Two summary figures of temperature results have been published previously. The review by Helz and others (2014a) included an overview of the thermal results for boreholes from the center of Kīlauea Iki lava lake, from 1962 through 1988; the summary figure is reproduced here as figure 13. Three types of data have been obtained: downhole thermocouple measurements, temperature estimates from coexisting magnetite and ilmenite (where present), and glass geothermometry (developed by Helz and Thornber, 1987). Figure 13 shows that these three types of data give broadly compatible results for the boreholes involved, and that the results give a reasonably complete picture of the thermal evolution of the upper crust and partially molten zone of the lava lake. An alternative presentation of cooling history is given in figure 14, which is similar to figure 4 in Barth and others (1994), with results from borehole KI88-2 added. This figure shows how the upper crust of the lava lake has thickened with time. It also suggests that the maximum temperature in the core of the lake dropped below the solidus (T~ 1,000 °C) in the 1990s. The purpose of the final section of this report is to present the background data for the temperature determinations and to show how the results dovetail for a wider range of boreholes than those included in figures 13 and 14.
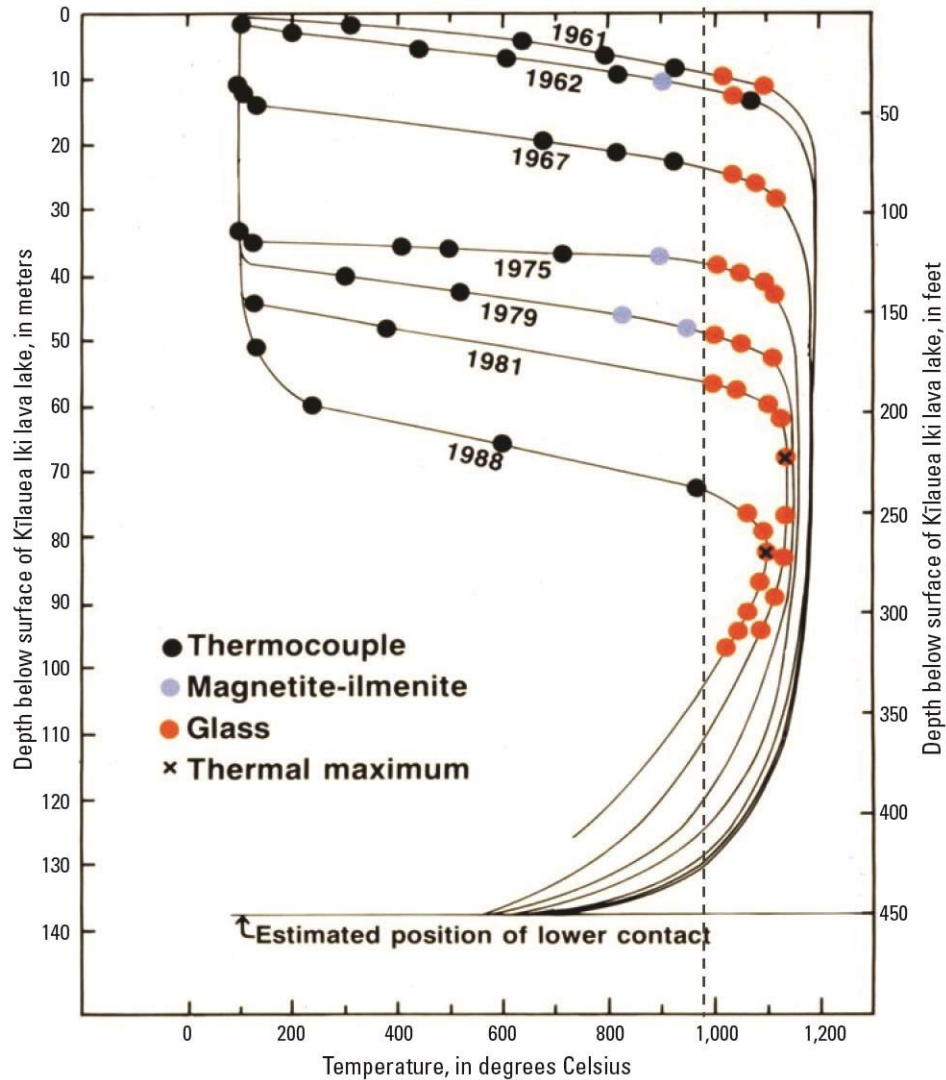
Figure 13. Graph showing variation of temperature with depth below the surface of Kīlauea Iki lava lake as a function of time, for boreholes and core from the center of the lake. Shapes of curves below ~100 meters (m) are constrained by an assumed depth of 135 m (Helz, 1993) and a lower contact temperature of ~600 °C, which is based on an initial lake temperature of ~1,190 °C (Helz, 2009). The dashed vertical line shows the approximate position of the solidus for the olivine-phyric matrix compositions. Modified from figure 16b in Helz and others (2014a).
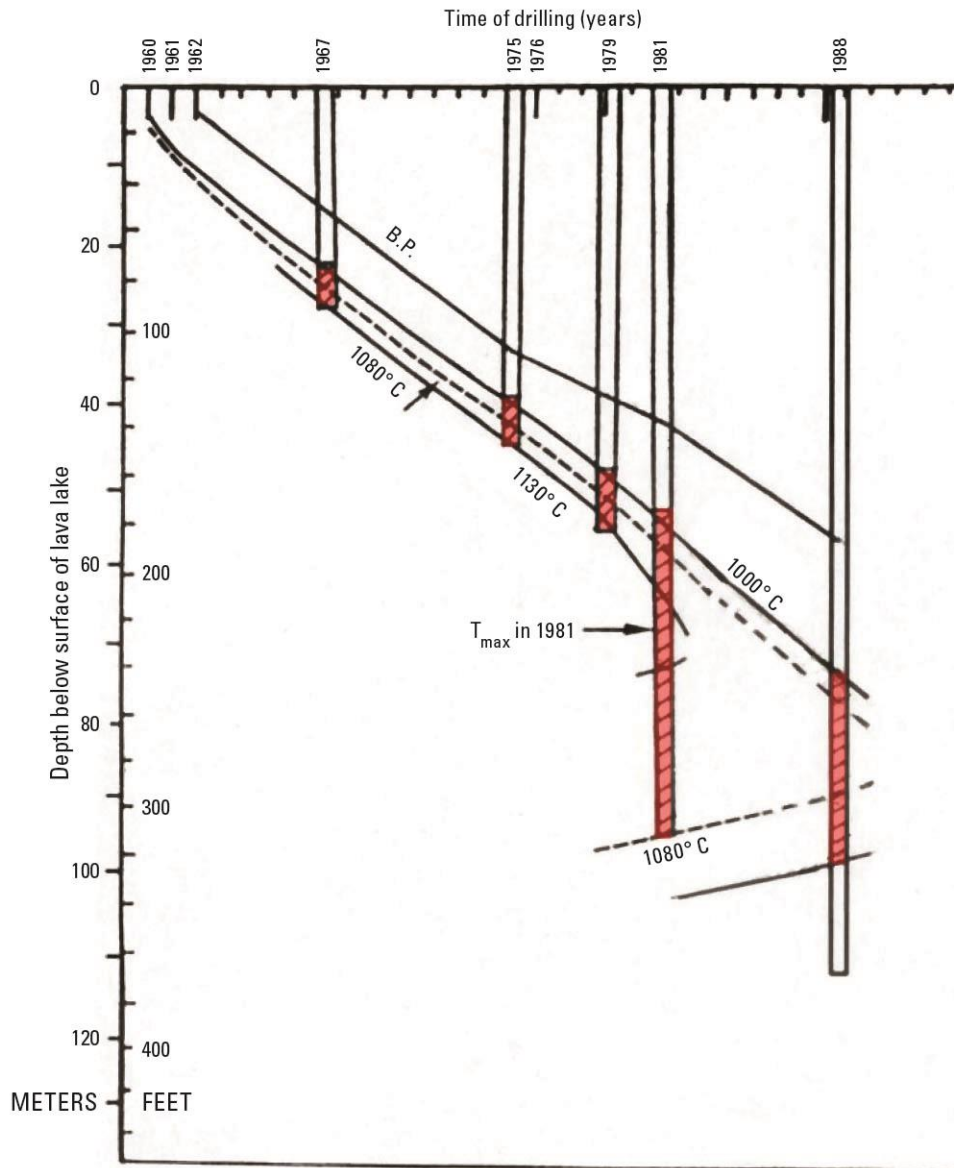
Figure 14. Graph showing how selected isotherms (temperature in degrees Celsius) shifted downward with time in boreholes from the center of Kīlauea Iki lava lake. The highlighted segments indicate core that was partially molten at the time of drilling. B.P. indicates the depth at which the temperature of the boiling point of water was reached.

Downhole Thermocouple Measurements

The earliest (1960–1962) drilling episodes were in all cases followed by downhole measurements of temperature, using Pt-Rh thermocouples; those data are given in Richter and Moore (1966). Similar observations were obtained for many of the holes drilled from 1967 to 1988. Appendix 2 includes all useful profiles obtained; most are released here for the first time. Previously published thermocouple profiles for these later Kīlauea Iki boreholes can be found in Hardee (1980), Hardee and others (1981), and Barth and others (1994).

Appendix 2 (tables 2.1–2.4) includes information on the date of completion of each hole, dates of the various thermocouple profiles made, and information on other aspects of the

25

operation, including identifying wherever possible the people who made the measurements (including Hawaiian Volcano Observatory scientists and staff, visiting scientists and students, and personnel from Sandia National Laboratories). Useful profiles were not obtained for every borehole: some holes were blocked by debris or backfilled by ooze at high enough levels that no temperatures higher than ~100 °C (the boiling point of the water in the geothermal system that was present in the upper crust of the lake) were measured. Where more than one profile was obtained for a given borehole, comparison of the profiles offers some insight into (1) how much post-drilling temperatures were affected by the cooling water used during drilling, (2) how quickly and to what extent the wall rock recovered after drilling, and (3) how quickly subsequent cooling took over, as the lake continued to cool. Further details on the format followed in appendix 2 and figures 15–22 are discussed below.

Fe-Ti oxide Assemblages and Oxide Geothermometry

The Fe-Ti oxide assemblages observed in Kīlauea Iki drill core were summarized in Helz (1987b). The first oxide to crystallize is always a high-Ti oxide: ilmenite ($FeTiO_3$) in much of the lake, but with ferropseudobrookite ($FeTi_2O_5$) either first, or shortly after ilmenite precipitation in the olivine-rich zone. Typical compositions are given in table 3. At an appreciably lower temperature, magnetite crystallizes along with ilmenite; selected data for coexisting magnetite-ilmenite pairs are presented in table 4. Additional data on Fe-Ti oxide compositions in Kīlauea Iki can be found in Greaney and others (2017).

Table 3. Compositions of first Fe-Ti oxide phases near their first appearance.

[Data in weight percent]

Sample no. and oxide phase	KI75-1-139.3 Ilmenite	KI75-3-145.7 Ilmenite	KI79-1-175.0 Ilmenite	KI79-1-175.0 Ferropseudo-brookite	KI79-3-171.9 Ilmenite	KI79-3-171.9 Ferropseudo-brookite	KI81-1-189.4 Ilmenite	KI81-1-189.4 Ferropseudo-brookite	KI81-1-294.9 Ferropseudo-brookite
Date analyzed	14 Jul 1987	22 Jun 1980	14 Jul 1987	14 Jul 1987	14 Jul 1987	14 Jul 1987	14 Jul 1987	14 Jul 1987	14 Jul 1987
No. points	3	2	1	1	1	2	3	1	1
TiO_2	47.96	47.11	48.70	62.05	49.21	62.53	48.80	61.09	62.92
Al_2O_3	0.54	0.53	0.68	1.80	0.63	1.88	0.59	1.63	1.90
Cr_2O_3	0.19	0.48	0.22	0.15	0.23	0.22	0.32	0.15	0.38
FeO(total)	44.61	41.38	42.09	27.78	41.85	27.90	42.43	29.97	27.09
MnO	0.20	0.31	0.20	0.10	0.21	0.15	0.18	0.16	0.13
MgO	6.11	7.09	7.32	6.39	7.67	6.63	6.74	5.68	6.92
Sum	99.61	96.90	99.21	98.27	99.80	99.31	99.06	98.68	99.34
T_{MgO} *	1,085	1,108	1,095	1,095	1,100	1,100	1,093	1,093	1,112
T_{CaO} *	1,084	1,106	1,094	1,094	1,097	1,097	1,092	1,092	1,108

*Glass quenching temperatures (degrees Celsius) from Helz and Thornber (1987).

Table 4. Analyses of ilmenite (Ilm)-magnetite (Mt) pairs used in temperature profiles.

[Analytical data in weight percent. Abbreviations: %, percent; usp, ulvospinel; T, temperature in degrees Celsius]

Sample no.	Date of analysis	Phase	TiO_2	Al_2O_3	Cr_2O_3	FeO (total)	MnO	MgO	Sum	Ilm (mol %)	Usp (mol %)	T[1]	log f_{O_2}[2]	T_{CaO}[3]	Comments
KI-227	23 Sep 1980	Ilm	49.53	0.13	0.09	47.16	0.60	1.33	98.84	94.7		895	−13.3	glass metastable	compound
		Mt	23.78	1.51	0.08	69.86	0.51	0.98	96.72		68.7				
KI-231	23 Oct 1980	Ilm 1	48.55	0.38	0.25	46.37	0.33	3.27	99.15	89.4		995	−10.8	1,007–1,010	adjacent + glass
		Mt 1	20.57	1.73	0.29	69.96	0.39	2.38	95.32		57.9				
KI-231	23 Oct 1980	Ilm 2	47.30	0.30	0.16	45.56	0.45	3.10	96.87	89.0		1,000	−10.8	1,007–1,010	adjacent + glass
		Mt 2	20.59	1.78	0.26	69.58	0.36	2.42	94.99		58.2				
KI75-1-125	23 Oct 1980	Ilm 1	50.05	0.23	0.25	47.04	0.61	1.58	99.76	93.8		910	−12.9	glass metastable	compound
		Mt 1	21.99	1.76	0.28	72.02	0.51	1.50	98.06		63.3				
KI75-1-125	23 Oct 1980	Ilm 2	49.45	0.27	0.00	47.00	0.61	1.64	98.97	93.1		915	−12.8	glass metastable	compound
		Mt 2	22.07	1.86	0.11	71.61	0.54	0.99	97.18		63.7				
KI75-1-125	23 Oct 1980	Ilm 5	49.35	0.34	0.25	47.37	0.55	1.35	99.21	93.2		890	−13.5	glass metastable	compound
		Mt 5	22.75	1.85	0.21	72.65	0.51	0.78	98.75		65.1				
KI75-1-128	23 Sep 1980	Ilm 1	48.20	0.16	0.04	47.83	0.55	1.30	98.08	91.7		1,000	−11.1	986–987	compound
		Mt 1	22.75	1.31	0.06	69.86	0.47	0.85	95.30		66.5				
KI75-1-128	23 Sep 1980	Ilm 2	48.77	0.20	0.00	48.03	0.61	1.44	99.05	91.7		995	−11.2	986–987	compound
		Mt 2	22.58	1.48	0.05	69.93	0.49	1.07	95.60		65.6				
KI75-1-128	23 Sep 1980	Ilm 3	48.26	0.22	0.05	46.96	0.57	1.49	97.55	92.3		970	−11.8	986–987	compound
		Mt 3	23.14	1.63	0.08	71.55	0.51	1.01	97.92		66.0				

28

Table 4. Analyses of ilmenite (Ilm)-magnetite (Mt) pairs used in temperature profiles.—Continued

[Analytical data in weight percent. Abbreviations: %, percent; usp, ulvospinel; T, temperature in degrees Celsius]

Sample no.	Date of analysis	Phase	TiO_2	Al_2O_3	Cr_2O_3	FeO (total)	MnO	MgO	Sum	Ilm (mol %)	Usp (mol %)	T[1]	log f_{O_2}[2]	T_{CaO}[3]	Comments
KI75-2-129.1	23 Sep 1980	Ilm 1	48.18	0.23	0.04	47.12	0.43	2.56	98.56	89.7		970	−11.3	985–990	compound
		Mt 1	19.56	1.49	0.14	72.25	0.40	1.65	95.49		55.4				
KI75-2-129.1	23 Sep 1980	Ilm 2	48.76	0.21	0.02	47.95	0.48	2.52	99.94	89.6		960	−11.3	985–990	compound
		Mt 2	19.68	1.38	0.15	73.50	0.37	1.58	96.66		55.0				
KI75-2-129.1	23 Sep 1980	Ilm 3	48.39	0.17	0.09	46.98	0.50	2.54	98.67	90.0		955	−11.4	985–990	compound
		Mt 3	19.11	1.34	0.29	71.94	0.29	1.60	94.57		54.8				
KI79-3-150.0	12 Mar 1981	Ilm 1	46.04	0.01	0.44	47.03	0.37	4.14	98.03	83.3		840	−11.8	no glass	adjacent
		Mt 1	8.64	1.76	0.11	82.06	0.28	1.76	94.61		22.2				
KI79-3-150.0	12 Mar 1981	Ilm 3	44.79	0.50	0.37	48.50	0.33	3.91	98.40	81.0		885	−10.9	no glass	adjacent
		Mt 3	9.34	1.97	0.21	81.24	0.27	1.92	94.95		24.1				
KI79-3-150.0	12 Mar 1981	Ilm 4	46.27	0.14	0.39	45.00	0.42	4.08	96.30	86.0		820	−12.5	no glass	adjacent
		Mt 4	9.25	1.72	0.55	81.84	0.28	1.89	95.53		23.8				
KI79-3-157.7	23 Oct 1980	Ilm 1	47.99	0.38	0.00	44.93	0.39	2.66	96.35	91.7		945	−11.8	glass metastable	compound
		Mt 1	20.61	2.58	0.22	71.29	0.35	1.83	96.88		59.3				
KI79-3-157.7	23 Oct 1980	Ilm 2	48.65	0.31	0.0	46.02	0.41	2.44	97.83	91.7		950	−11.7	glass metastable	compound
		Mt 2	21.31	1.63	0.31	71.82	0.34	1.78	97.19		60.1				
KI79-3-157.7	12 Mar 1981	Ilm 3	48.34	0.22	0.33	46.71	0.39	2.60	98.59	90.3		960	−11.5	glass metastable	compound, next vein
		Mt 3	19.77	2.69	0.05	73.68	0.34	1.86	98.39		55.6				

29

Table 4. Analyses of ilmenite (Ilm)-magnetite (Mt) pairs used in temperature profiles.—Continued

[Analytical data in weight percent. Abbreviations: %, percent; usp, ulvospinel; T, temperature in degrees Celsius]

Sample no.	Date of analysis	Phase	TiO$_2$	Al$_2$O$_3$	Cr$_2$O$_3$	FeO (total)	MnO	MgO	Sum	Ilm (mol %)	Usp (mol %)	T[1]	log f$_{O2}$[2]	T$_{CaO}$[3]	Comments
KI79-5-145.7	30 Jun 1981	Ilm 1	43.06	0	0.04	50.51	0.57	2.83	97.01	79.2		830–835	−11.2	no glass	compound
		Mt 1	6.20	1.60	0.29	84.62	0.20	1.10	94.01		16.5				
KI79-5-145.7	30 Jun 1981	Ilm 2	42.40	0.0	0.01	48.82	0.55	3.32	95.10	78.7		815	−11.2	no glass	compound
		Mt 2	5.43	1.15	0.08	82.46	0.34	1.36	90.82		13.54				

[1]Temperature (degrees Celsius) calculated from oxide pairs (Buddington and Lindsley, 1964).

[2]Log f$_{O2}$ is the log of the oxygen fugacity calculated from oxide pairs (Buddington and Lindsley, 1964).

[3]Glass quenching temperature (degrees Celsius) from Helz and Thornber (1987).

No temperature estimates can be made based on the composition of ilmenite ± ferropseudobrookite. However, pioneering work by Buddington and Lindsley (1964) established the possibility of obtaining both an equilibration temperature and an estimate of oxygen fugacity from coexisting pairs of magnetite and ilmenite. Accordingly, from 1980 to 1981, electron microprobe analyses of coexisting magnetite-ilmenite pairs were made in as many Kīlauea Iki drill core samples as possible. The microprobe techniques used were as described above, though with appropriate oxide standards. The analyses were reduced and the percentages of ilmenite ($FeTiO_3$) and ulvospinel (Fe_2TiO_4) calculated following the method of Anderson and Wright (1972).

A limitation of the Fe-Ti oxide geothermometry was that the desired information on temperature can be obtained only for temperatures below the incoming of magnetite (~1,070 °C), as both ilmenite (which begins to crystallize at ~1,105 °C) and the spinel phase must be present and in physical contact for the method to be applied. This method has been useful chiefly in constraining the temperatures of 1962–1979 drill core from the lowest part of the crystallization range and from the high subsolidus region. Table 4 gives the results for all Fe-Ti oxide pairs that usefully complement other methods of obtaining temperature information. Note that almost all the pairs are from compound grains, and the few described as adjacent grains were almost touching. Data shown in the figures discussed below are average temperature values with an uncertainty bracket of ±50 °C (Buddington and Lindsley, 1964).

Glass Geothermometry

The principal method for establishing quenching temperatures of Kīlauea Iki drill core has been glass geothermometry (Helz and Thornber, 1987). This method, based on melting experiments on Kīlauea Iki samples (phase compositions in appendix 1, tables 1.10–1.13), allows the use of (1) the MgO content of glass in equilibrium with olivine (T_{MgO}) or (2) the CaO content of glass in equilibrium with olivine + augite + plagioclase (T_{CaO}) to estimate the quenching temperature of almost all glassy core samples. In that paper, Helz and Thornber presented temperature profiles for almost all the glassy drill cores available to date. Since then, the method has also been applied to glassy samples from the 1988 cores. Resulting temperature estimates [all in degrees Celsius (°C)] for all samples are given in appendix 1, table 1.1.

Notes on the Thermal Data in Appendix 2 and in Figures 15–22

Appendix 2 presents all useful thermocouple profiles taken in boreholes in Kīlauea Iki lava lake, as follows: data for the 1967 holes are in appendix table 2.1, for the 1975 holes in table 2.2, for the 1976 and 1979 holes in table 2.3, and for the 1981 and 1988 holes in table 2.4. The thermocouple data were obtained over the period 1967 to 1989 through the efforts of scientists and staff of the Hawaiian Volcano Observatory (HVO), with occasional help from visiting scientists. HVO personnel included L.A. Anderson, R.S. Fiske, T.L. Wright, R.T. Okamura, A. Yamamoto, M.K. Sako, K.M. Yamashita, D.A. Swanson, R. Mitchell, R.I. Tilling, T.J. Casadevall, N.G. Banks, and M.T. Mangan. Visitors helping with the measurements included M. Coltelli (Istituto Nazionale di Geofisica e Vulcanologia, Catania, Italy) and L. Kestay (California Institute of Technology). In addition, special thanks are extended to M.P. Ryan (then University of Hawaii at Manoa) and to J.L. Colp and R.G. Hill (Sandia National Laboratories) for sharing thermocouple data for the 1979 and 1981 boreholes.

Profiles are presented in paired columns with depth (in feet) in the first column and temperature (in degrees Celsius) in the second column. Headers for each pair include (1) the number of the borehole, (2) the date its drilling was completed, (3) the date the thermocouple profile was taken, and (4) the names of the above-mentioned scientists who made the measurements in the individual profiles.

The profiles themselves begin with the depth to the bottom of the hole as drilled and the temperature originally found at that depth. That temperature is usually from glass geothermometry (Helz and Thornber, 1987), as any hole that penetrated the partially molten zone in the lake was backfilled by melt oozing into the open, uncased borehole. The bottom of the hole as found on the day the profile was taken is then noted, together with the glass geothermometry temperature at that depth. All glass geothermometry values are in boldface in appendix 2.

Below those data, the tables contain the temperatures recorded by thermocouple measurements at a given depth. For the 1967 to 1979 holes, measurements were taken from the bottom of the hole up, as noted in the spreadsheet. In 1981–1988, profiles were taken either from the top down or both up and down (as in the 1988 boreholes in table 2.4). In all cases, the shallowest part of the temperature profile reported temperatures close to the boiling point of water (~100 °C), which did not vary with depth. These steep profiles result from convection of liquid water and steam in the uncased boreholes.

Other annotations in appendix 2 include notes for profiles indicating that they were "pre-drilling," that is, taken before the hole had reached its maximum depth. Most profiles are post-drilling, taken some time after the hole was completed. For the most part, temperature increases steadily with depth in the hole. However, a few profiles show local reversals in temperature, and these, which were always checked and confirmed in the field, have been flagged in the tables. Finally, for any hole that passed through the thermal maximum (T_{max}), its position and the glass geothermometry value at that depth have been noted, adjacent to the profiles, at roughly the depth of T_{max}.

The section below presents a series of figures (figs. 15–22) with two to four different kinds of temperature information for each individual borehole. The notations used are (1) T_{MgO} and T_{CaO} for glass geothermometry results as shown in table 1.1, (2) t.c. for thermocouple measurements as shown in tables 2.1–2.4, and (3) temperatures for coexisting Fe-Ti oxides, as shown in table 4. All temperatures (T) are in degrees Celsius in these figures and throughout this report. In many cases, the thermocouple (t.c.) profiles are labeled with the date on which they were taken, as shown in appendix 2. This is to make clear, where the appendix contains more than one profile for a given hole, which profile has been used in the figure.

Comparative Geothermometry for Individual Cores from Kīlauea Iki Lava Lake

This section presents compound temperature profiles for each Kīlauea Iki borehole and core for which more than one type of temperature data is available. Previously published profiles included mostly glass geothermometry results (Helz and Thornber, 1987) or results for only selected locations (Barth and others 1994; Helz and others, 2014a). The figures included here focus mostly on data from 500 to 1,200 °C, so they are more detailed than the profiles in figure 13 and allow one to evaluate better how the different methods mesh with each other.

As already shown in Helz and Thornber (1987), the two glass geothermometers give similar results for most of the glasses from the lava lake. [This is in contrast to eruption glasses from Kīlauea, where T_{CaO} generally lags behind T_{MgO} (Helz and others, 1995)]. An unexpected result of using the glass geothermometry was that glass compositions appear to track predrilling temperatures well below the end of the experimental calibration (at 1,060 °C). This can be seen in compound curves like those in figure 13, where the overall shapes of the temperature profiles match those predicted from conductive cooling models (Helz and others, 2014a). This may be because, in the Kīlauea Iki magma (a low-silica tholeiite), olivine persists as a groundmass phase in all matrix samples, including those quenched below the solidus (Helz and others, 2014a). The results in figures 15 to 22 show that T_{MgO} tracks temperature fairly well to 1,030–1,044 °C (MgO = 0.9–1.6 weight percent), and that T_{CaO} tracks temperature to 986–1,018 °C (CaO = 1.5–3.0 weight percent) for cores recovered between 1967 and 1988. Accordingly, in those figures, temperature values that track predrilling temperatures are connected by solid lines. For data points connected by dotted lines, the residual rhyolitic glass could not and did not change composition with temperature, and therefore is considered to have been metastable (see discussion below).

Data from 1962 and 1967 boreholes and cores are summarized in figure 15. At that time, boreholes were blocked by melt at fairly shallow depths, so the total amount of cooling water used to produce the holes and recover the core was comparatively small. Also, the 1967 holes were drilled in stages (Helz and others, 1984); thus, two of the thermocouple profiles shown (for KI67-1 and KI67-3) were taken just before the final day of drilling. Consequently, the thermocouple profiles and the glass geothermometry results are very close to each other, though with less overlap than the data from the 1962 borehole. The limited Fe-Ti oxide data are consistent with the other two methods.
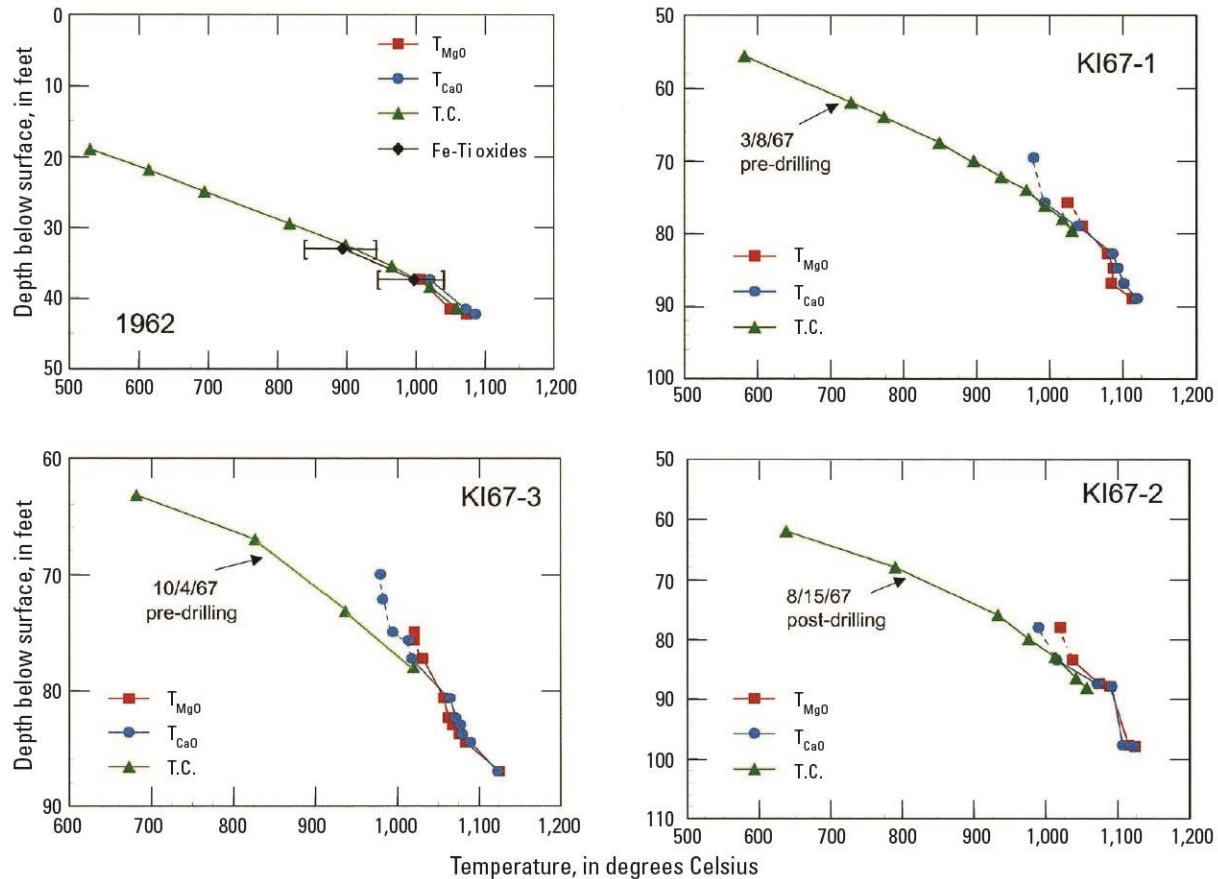
Figure 15. Graphs showing temperature variation with depth below the surface of Kīlauea Iki lava lake in four boreholes and cores from 1962 and 1967. The brackets on temperatures from Fe-Ti oxide pairs are ±50 °C. Dashed lines indicate that the rhyolitic residual glass is metastable in these samples. The 1962 data are from Richter and Moore (1966). The 1967 data are from appendix tables 1.1 and 2.1, plus table 4 in the text. See text for discussion.

By 1975–1976, the partially molten zone was twice as deep, so more cooling water was needed and the effects on post-drilling temperatures in the boreholes were larger than in the earlier holes. All thermocouple profiles were taken after completion of the holes, and for KI76-1 the profiles were taken after the drilling of a second hole (KI76-2), which was 1.2 ft (0.36 m) away from KI76-1. The thermocouple profiles selected for figure 16 are the hottest (best recovered) profiles available, but the holes were blocked by ooze (Helz and others, 1984); thus the thermocouple profiles do not extend to the original bottom of the holes. Nevertheless, the thermocouple data lie close to the glass data, and the shape of the thermocouple profiles parallels the shape of the glass geothermometry profiles. Oxide data, where available, are broadly consistent with the glass results, and so give an indication of where temperatures in the high subsolidus range fell (see oxide slopes for KI75-1 and KI76-1) prior to drilling.
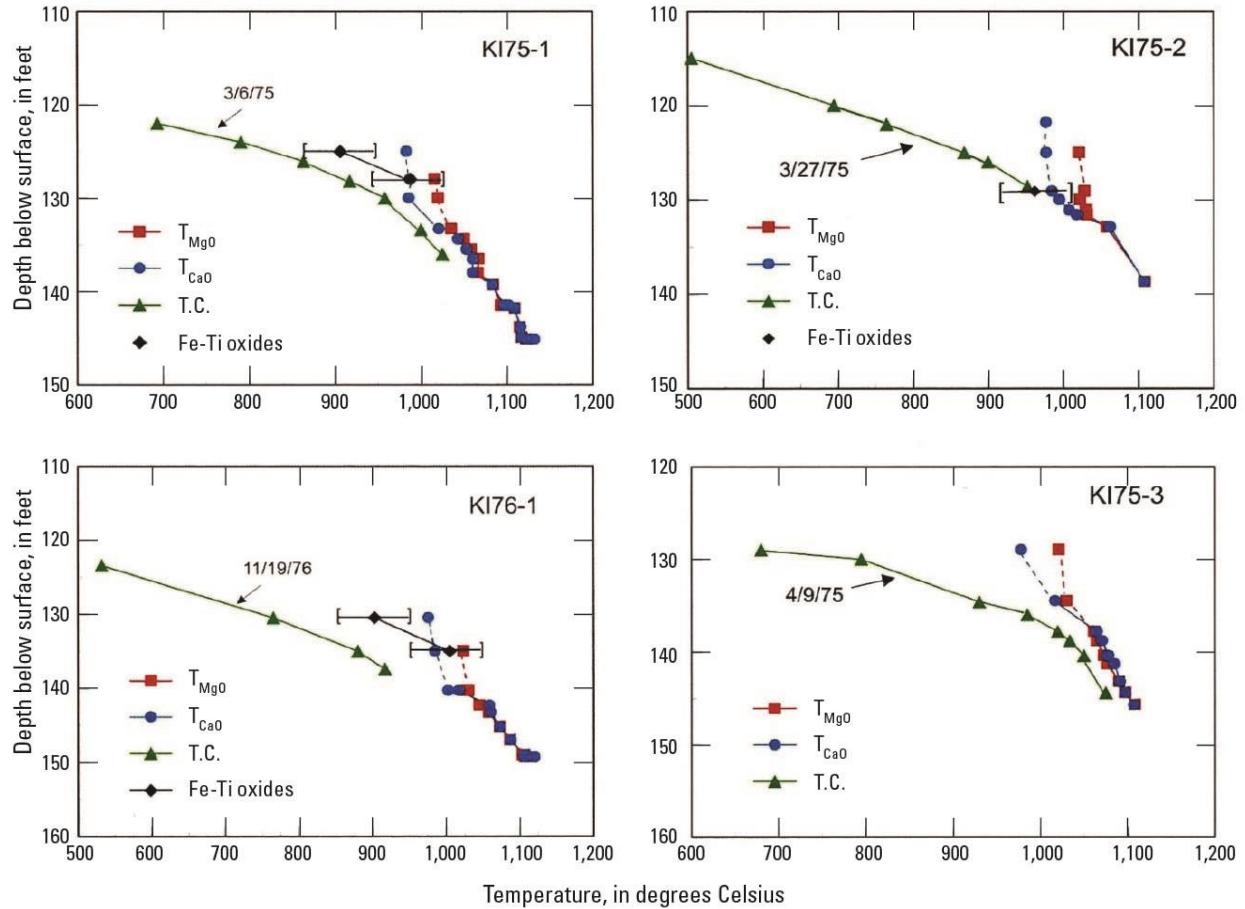
Figure 16. Graphs showing temperature variation with depth below the surface of Kīlauea Iki lava lake in four boreholes and cores from 1975 and 1976. The brackets on temperatures from Fe-Ti oxide pairs are ±50 °C. Dashed lines indicate that the rhyolitic residual glass is metastable in these samples. Data are from appendix tables 1.1 and 2.2–2.3, plus table 4 in the text. See text for discussion.

Figure 17 presents data from two 1979 boreholes. The thermocouple profile for KI79-3 is low relative to the other data, as this profile was taken after three holes had been drilled nearby: KI75-1R, KI79-3, and KI79-4 (Helz and others, 1984). Thus, the best thermal recovery seen is relatively poor. Note that the results for the Fe-Ti oxides are consistent with the glass geothermometry, not with the thermocouple data. For KI79-6, there are no useful thermocouple profiles, but as for KI79-3, the slopes for Fe-Ti oxide and glass geothermometry data compare reasonably well.
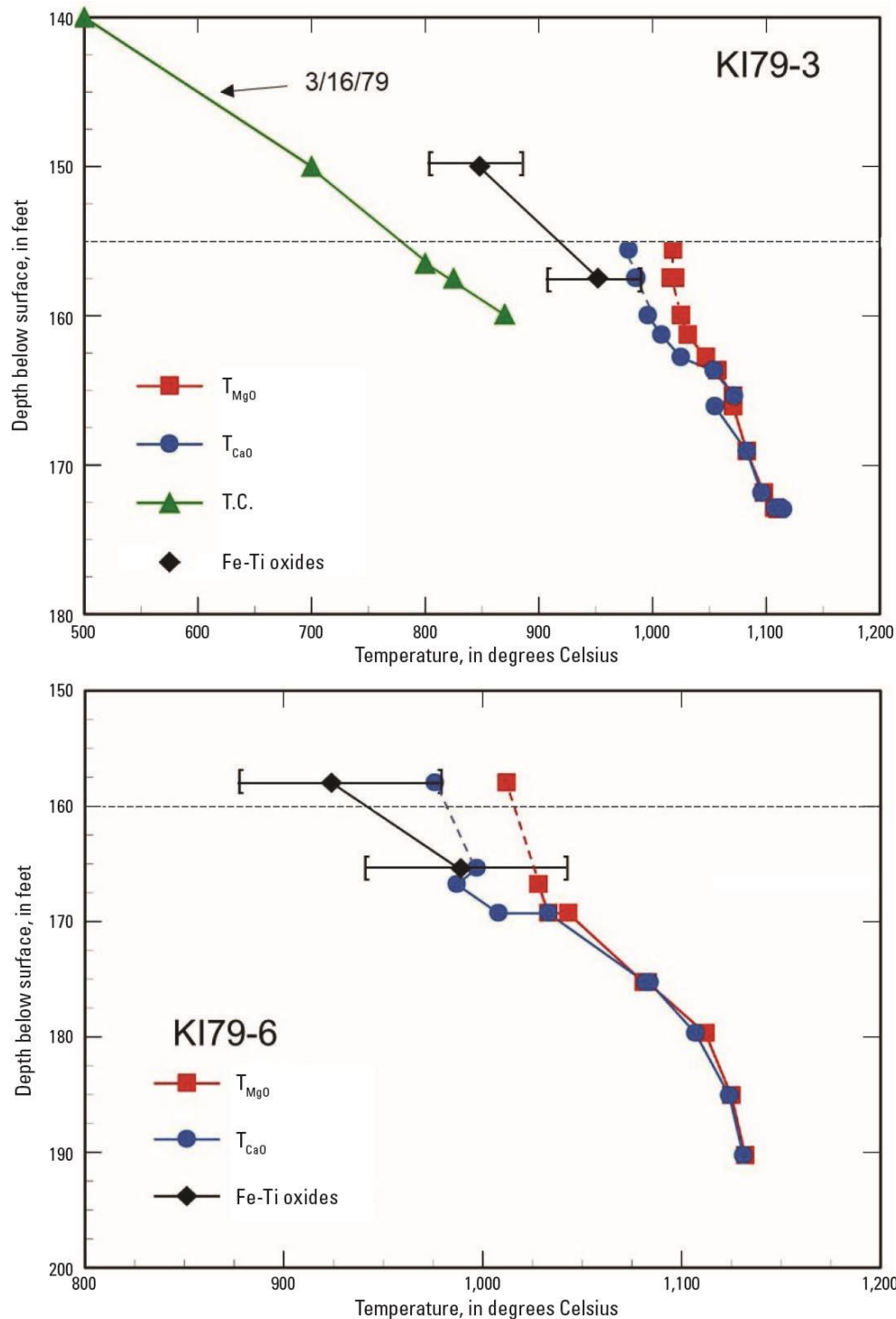
Figure 17. Graphs showing temperature variation with depth below the surface of Kīlauea Iki lava lake in boreholes KI79-3 and KI79-6. Note the change in temperature scale for KI79-6. The horizontal dashed lines indicate the depth at which hackly radial fractures were first observed in these drill cores. The brackets on temperatures from Fe-Ti oxide pairs are ±50 °C. Dashed lines indicate that the rhyolitic residual glass is metastable in these samples. Data are from appendix tables 1.1 and 2.3, plus table 4 in the text. See text for discussion.

36

Borehole KI79-1 (fig. 18) has a double set of data: it was first drilled to 204 ft (62.2 m) but was abandoned because it did not "hit melt" (Helz and others, 1984). A thermocouple profile taken the next day (12/22/78; see appendix 2, table 2.3) showed that the hole was still completely open, and the shape of that profile was similar to the shape defined by T_{MgO} and T_{CaO} for the original core recovered. However, the hole collapsed and (or) backfilled gradually over the next 16 days, so that a thermocouple profile taken on January 6, 1979, extended to only 167 ft (50.9 m). The hole was repeatedly re-entered on January 25, 1979 (Helz and others, 1984), and a set of complexly differentiated oozes was recovered. The T_{MgO} and T_{CaO} profiles of the first-pass ooze recovered lie exactly on the extension of the 1/6/79 thermocouple profile, as was seen in comparing thermocouple and glass geothermometry results in the earliest boreholes (fig. 15).
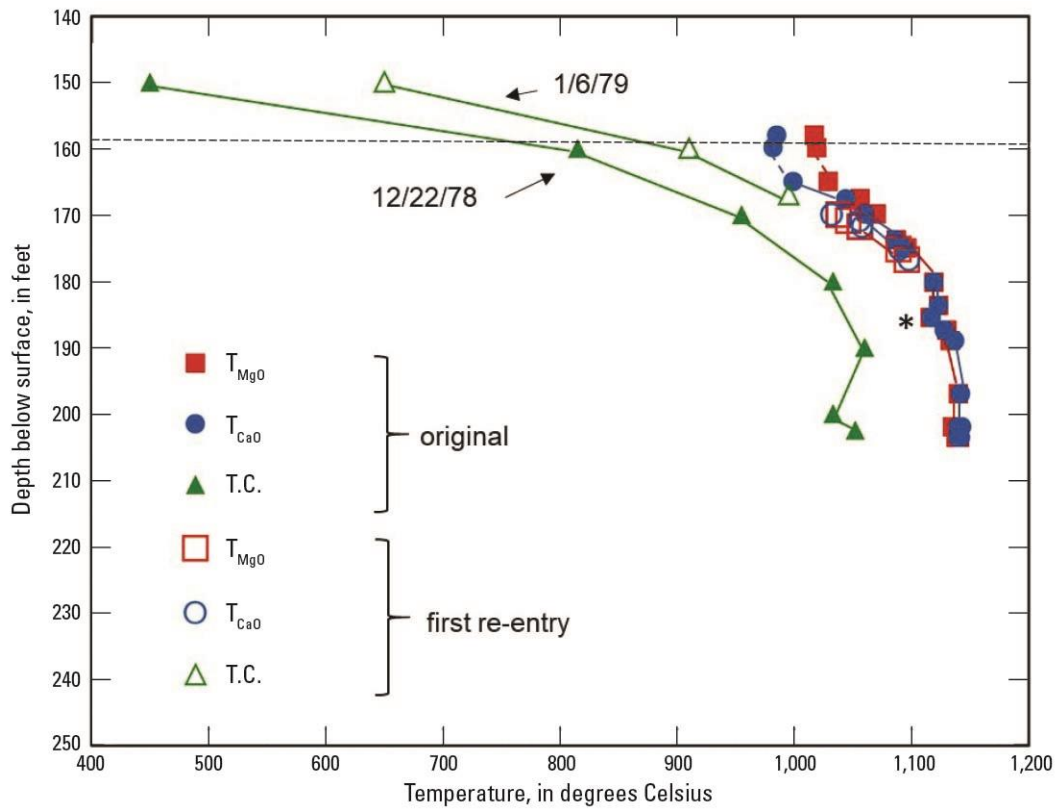

Figure 18. Graph showing temperature variation with depth below the surface of Kīlauea Iki lava lake in borehole KI79-1. Solid symbols indicate temperatures measured one day after the hole was completed, plus glass quenching temperatures observed in the initial core recovered. Open symbols show temperatures measured 16 days later, prior to re-entry of the hole, and the glass quenching temperatures are those observed in the ooze recovered during the first re-entry. The asterisk marks the position of the last overnight stop during initial drilling. The horizontal dashed line indicates the depth at which hackly radial fractures were first observed in the drill core. Dashed lines indicate that the rhyolitic residual glass is metastable. Thermocouple profiles (Colp, 1979) are in appendix table 2.4. The glass geothermometry data are from appendix table 1.1. See text for discussion.

Most of the 1981 boreholes were used for various geophysical and heat extraction experiments by personnel from Sandia National Laboratories, and assorted instruments and other debris were left in the holes (Helz and Wright, 1983), so there are only two thermocouple profiles available: one for KI81-1 (fig. 19 and appendix 2, table 2.4) and one for KI81-2 (fig. 20 and appendix 2, table 2.4). Figure 19 shows the available thermal data for KI81-1, for the temperature range between 0 °C and 1,200 °C. The glass results give a coherent picture of the temperature distribution in the partially molten zone, and the location of the Na_2SO_4 deposits in the core (see table 5, this report; descriptions in Helz and Wright, 1983) shows the position of the base of the geothermal system. The thermocouple profile is consistent with most of these data. However, it was taken while borehole KI81-5 was being drilled, about 30 ft (9 m) away. The curious excursion at T~400 °C (also shown in Hardee and others, 1981) was most likely caused by this adjacent drilling activity. Data on drill core from KI81-5 (see p. 17) suggest that its core was affected by the prior drilling of KI81-1 and the suite of engineering experiments carried out in that first hole. Thus the effects of cooling water used during drilling appear to extend sideways in the lava lake, over as much as 30 ft (9 m).
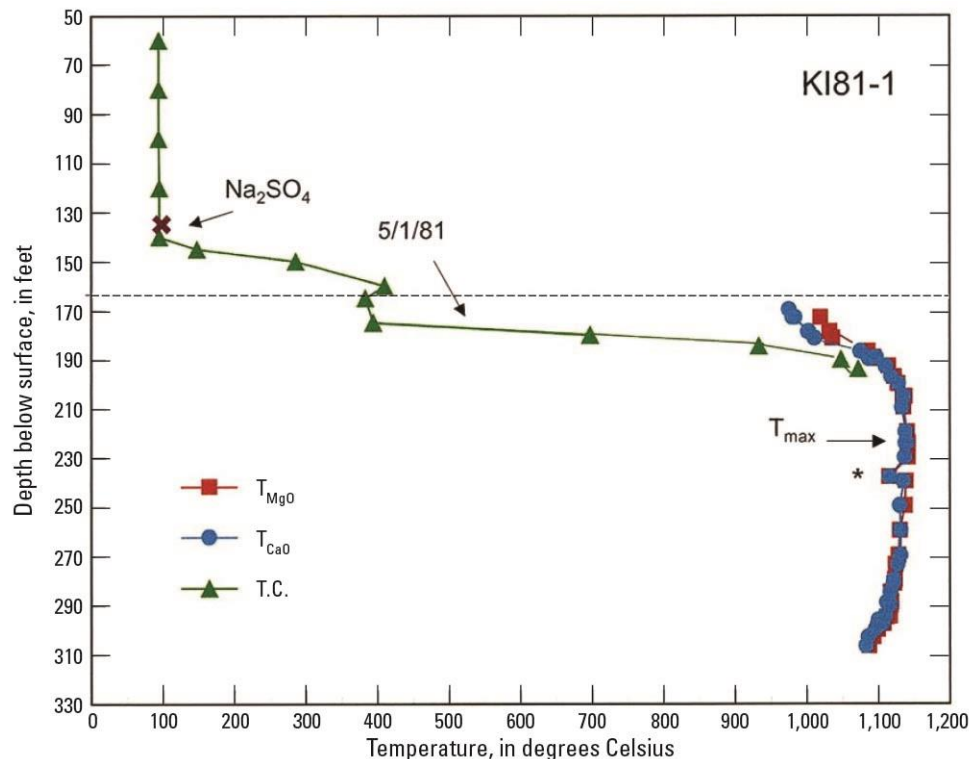

Figure 19. Graph showing temperature variation with depth below the surface of Kīlauea Iki lava lake in borehole KI81-1, which passed through the thermal maximum at 225 feet and penetrated the lower crust of the lava lake. The horizontal dashed line indicates the depth at which hackly radial fractures were first observed in the drill core. Asterisk marks the position of the last overnight stop during drilling. Note that the temperature scale extends to zero. The "**x**" shows the depth of the Na_2SO_4 deposit that marks the position of the base of the two-phase geothermal system in the upper crust of the lava lake. Data are from appendix tables 1.1 and 2.4, and table 5 in the text. See text for discussion.

Table 5. Available observations on location of Na_2SO_4 deposits versus the depth to the boiling curve in Kīlauea Iki drill cores.

[Temperature data from appendix 2. Abbreviations: T, temperature; °C, degrees Celsius]

Drill core	Depth of Na_2SO_4 deposits (feet)	Reference (USGS Open-File Report)	Depth to T ≥100 °C (feet)	Temperature at depth of deposits, where T >100 °C
KI67-1	not noted		18	
KI67-2	not noted		21	
KI75-1	105–114	84–484	110	
KI75-3	111–116	84–484	110	
KI76-1	109.5–110.5	84–484	105	
KI79-1	120–122	84–484	~110	
KI79-3	119–125	84–484	110	
KI79-5	124–134	84–484	<40–60	360–430 °C
KI79-6	120–148	84–484	no data	
KI81-1	134.7–137.7	83–326	140	
KI81-2	147.6	83–326	155	
KI81-3	145.3–146.0	83–326	no data	
KI81-6	143–146	83–326	no data	
KI88-1	209–210	93–15	<170	422 °C
KI88-2	182–191	93–15	<125	190–220 °C

Glass geothermometry in figure 20 shows that the profiles for KI81-2 and KI81-3 are similar to that for KI81-1, demonstrating that the partially molten mush zone was laterally coherent in size and temperature for ~500 ft (~150 m) along the north-south line of drilling in the lava lake (fig. 2). However, the thermocouple profile in KI81-2, taken the same day as the KI81-1 profile but about 100 ft (~30 m) to the north, is quite different. First it shows no reversal (appendix 2, table 2.4); this suggests that the effects of lateral migration of the cooling water were confined to the closely spaced clusters of holes seen in figure 3. However, because the KI81-2 profile was taken after that hole had been used for a heat extraction experiment (Helz and Wright, 1983), the temperatures observed are much lower than the original glass geothermometry results.
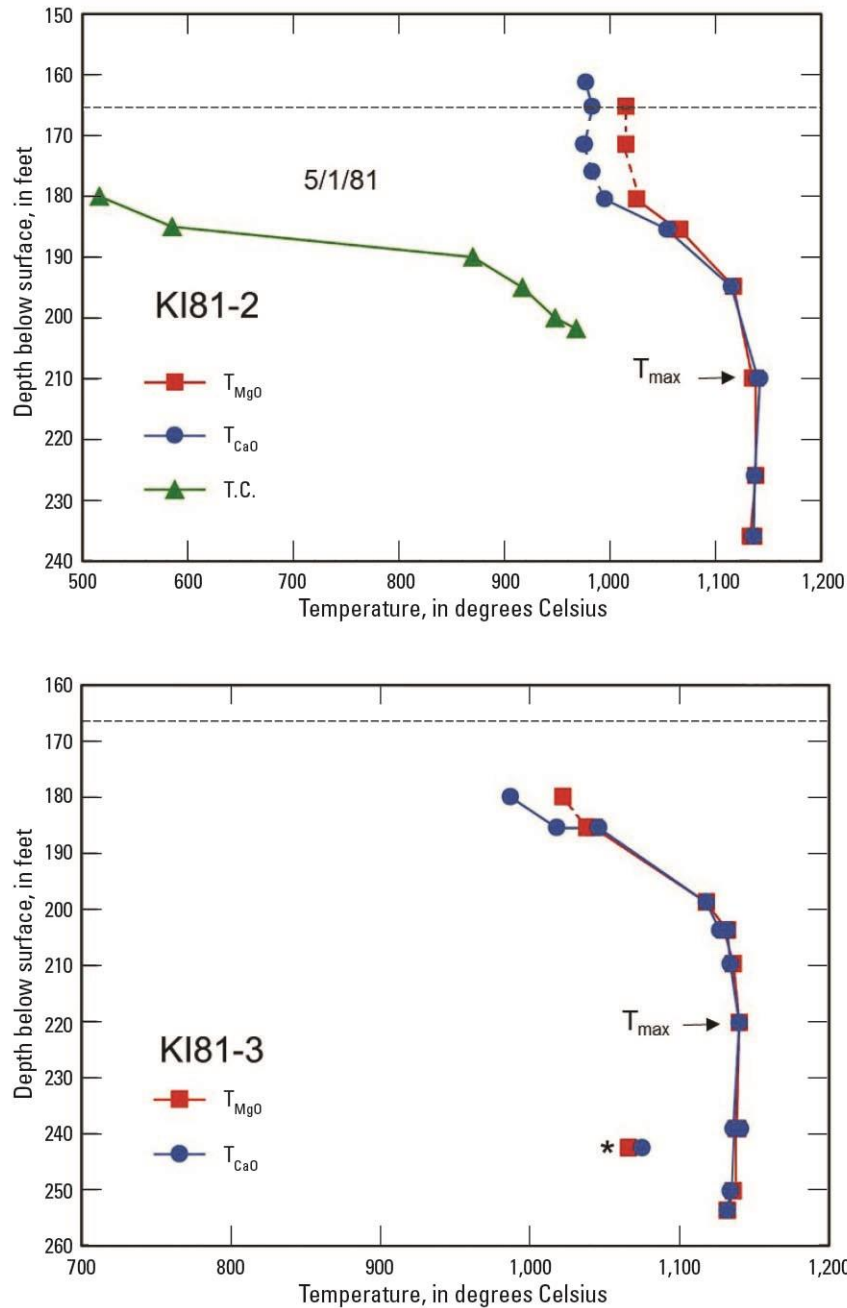
Figure 20. Graphs showing temperature variation with depth below the surface of Kīlauea Iki lava lake in boreholes KI81-2 and KI81-3. Both boreholes passed through the thermal maximum at the depths indicated, so that the lower parts of the curves are in the lower crust of the lava lake. Note the change in temperature scale for KI81-3. The horizontal dashed lines indicate the depth at which hackly radial fractures were first observed in the drill core. Dashed lines indicate that the rhyolitic residual glass is metastable in these samples. Asterisk in KI81-3 plot marks the position of the last overnight stop during drilling. Data are from appendix tables 1.1 and 2.4. See text for discussion.

Temperature Profiles in the Three Deepest Holes

All of the boreholes examined so far terminated within the partially molten core of Kīlauea Iki lava lake. Though mostly uncased, they did not experience major convection or heat transport up or down the holes, so the results of the thermocouple measurements are congruent with the results from glass and Fe-Ti oxide geothermometry, and in some cases directly coincide with those results. However, the three deepest holes drilled in the lake, which passed through the partially molten core into subsolidus crust below, show considerable divergence between the shape of the thermocouple profiles and other thermal data.

Part of the evidence for this divergence is summarized in table 5, which gives the available information on all drill cores where we have either (1) notes on the occurrence of Na_2SO_4 deposits in the core or (2) thermocouple profiles that show where the downhole temperature first exceeds the boiling point of water. Where both types of data are available, table 5 shows that the Na_2SO_4 deposit occurs at or slightly deeper than the depth to boiling, so is a reliable indicator of the position of the base of the two-phase geothermal system in the upper crust of the lava lake (as in KI81-1; see figure 19).

The first of the three deepest holes (KI79-5), drilled near the north edge of the lava lake, passed entirely through the lava lake (fig. 3). Temperature data bearing on the predrilling temperature distribution in this hole (fig. 21) include (1) a narrow range (163–194 ft or 49.7–59.1 m) of core that contains a residual rhyolitic glass, (2) two Fe-Ti oxide pairs that give temperature estimates supporting the glass results, and (3) a well-defined Na_2SO_4 deposit at a depth of 124–134 ft (37.8–40.8 m) as shown in table 5. These data combine to give a curve with a vertical convective profile to ~135 ft (41 m) like those seen in almost all thermocouple profiles in appendix 2, a steep rise to ~1,000 °C by 163 ft depth (49.7 m), and a gradual decline in temperature below 194 ft depth (59 m). The lower part of the predrilling curve (fig. 21) has been drawn to pass through T = 550 °C at the lower contact of the lake (313 ft, or 95.4 m). This temperature at the lower contact is what would be predicted from conductive cooling, which was the process by which the lava lake cooled (Helz, 1993, Helz and others, 2014a).

Because so little melt remained near the margin of the lava lake, borehole KI79-5 stayed open and could be re-entered over its entire depth. Two of the hottest thermocouple profiles through the lake are shown in figure 21. Although there is no reason to doubt the accuracy of the measurements, the shapes of the profiles are conspicuously different from the curve based on the other observations, as well as differing from each other. The area to the left of the three curves is similar, but the shapes of the profiles are grossly different. This is interpreted as resulting from the upward convection of steam and air in the open, uncased borehole: the borehole acted as a chimney, with the upper part of the hole experiencing temperatures well above 100 °C at depths previously occupied by the two-phase geothermal system (compare figure 21 and table 5). Note that the later profile shows better recovery of predrilling temperatures in the deepest part of the lava lake, though neither profile shows complete recovery.
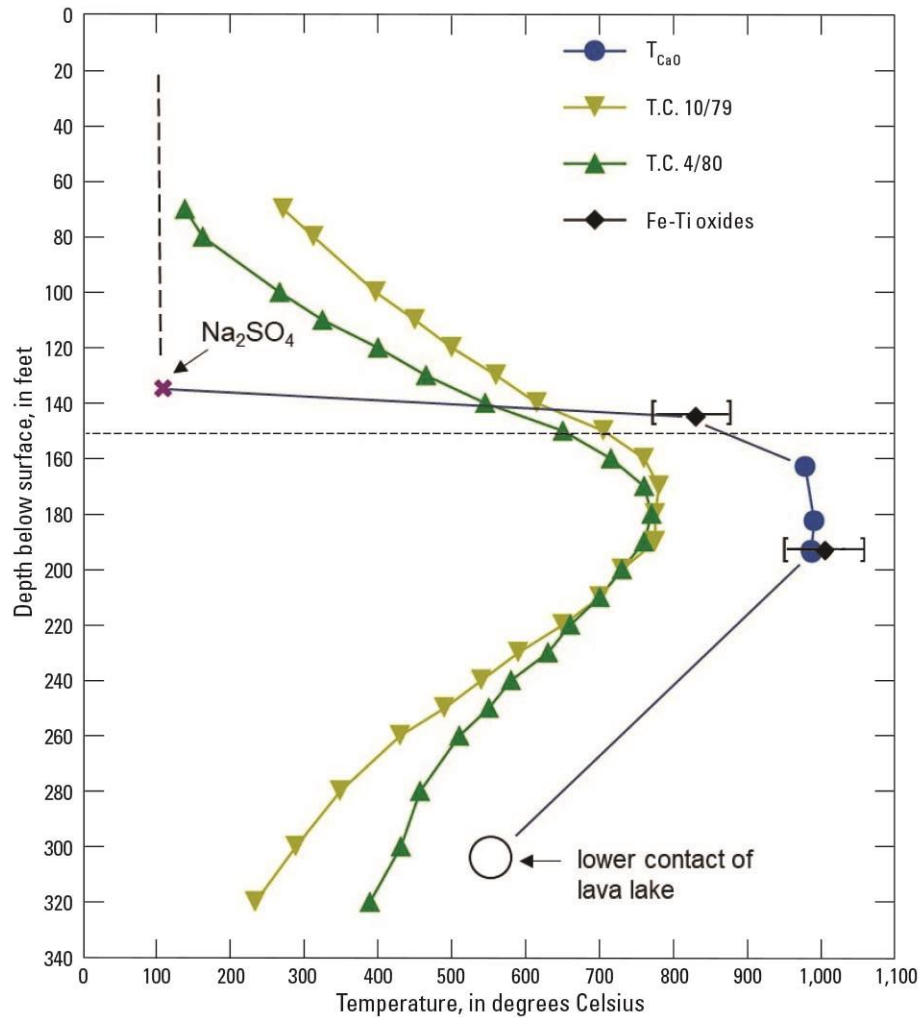
Figure 21. Graph showing available temperature constraints for borehole KI79-5, the only borehole that passed completely through Kīlauea Iki lava lake (lower contact shown in figure 3). The horizontal dashed line indicates the depth at which hackly radial fractures were first observed in this drill core. The brackets on temperatures from Fe-Ti oxide pairs are ±50 °C. All post-drilling thermocouple profiles have been affected by convection in the uncased borehole, so they are grossly different from the inferred predrilling temperature profile. Data are from appendix tables 1.1 and 2.3, plus tables 4 and 5 in the text. See text for discussion.

The final drilling of Kīlauea Iki took place in 1988, producing two boreholes that are deeper than any others (see figure 3). These did not reach the lower contact of the lake, but both reached the lower colonnade fracture set (see figure 4 in Helz, 1993), so they opened up pathways for convection of hot gases through the entire lava lake. Thermal data for the 1988 holes (fig. 22) include the available glass geothermometry (very limited for KI88-1) and two temperature profiles for each borehole. The shapes of the upper parts of thermocouple profiles resemble profiles in earlier boreholes (see figures 15–16, 18–19), at least down to the thermal maximum (T_{max}). There is a steep section from the surface to a certain depth, followed by a rapid increase in temperature to T_{max}, but with thermocouple measurements in the partially molten zone falling below the glass geothermometry data. However, table 5 shows that the Na_2SO_4 deposits, which mark the predrilling position of the base of the two-phase geothermal system, were observed at 182–191 ft (55.5–57.6 m) depth in borehole KI88-2 (where the thermocouple data showed T ~ 190–220 °C) and were found at 209–210 ft (63.7–64.0 m) in borehole KI88-1 (where the thermocouple data showed T = 422 °C). As in KI79-5, there has been some migration of heat up these boreholes, rewarming parts of the crust that had been at ~100 °C for years prior to drilling.

The most peculiar aspect of the 1988 thermocouple profiles vis à vis the glass geothermometry is seen in the region below the thermal maximum. Below T_{max}, the thermocouple temperatures curve sharply down for 20 to 30 ft (6–9 m), and then drop almost vertically to the bottom of the holes, *at higher temperatures than observed in the original cores*. In KI88-2, T ~ 1,030 °C in this vertical section, down to 354 ft (107.9 m), while the original core is subsolidus (T ~ 1,000 °C) below ~326 ft (99.4 m). In hole KI88-1, the thermocouple profiles hover at the solidus temperature down to the bottom of the hole (376 ft or 114.6 m), while the core is subsolidus below ~310 ft (94.5 m). The steepness of the curves is consistent with convection of hot gases in the borehole, but it is not clear why the lower parts of these holes are being reheated. Whatever the pattern of convection in the holes, it should be emphasized that the two sets of thermocouple measurements are reproducible within each hole, and were taken over a period of several days, so these peculiarities appear not to reflect problems during measurement.

Metastable Glasses in Drill Cores

Strictly speaking, all glasses are metastable at ambient temperatures. However, it was noted above (p. 33) that the glass geothermometers appear to track changes in temperature down to 1,030–1,044 °C (T_{MgO}) and down to 986–1,018 °C (T_{CaO}). Glasses exhibiting this behavior are interpreted as having been stable liquids prior to drilling and have been connected in figures 15–22 by solid lines. There is a second population of glasses (analyzed in most of the 1967 to 1981 cores), which have been identified in the appendix tables as "metastable." These rhyolitic glasses are marked by dashed rather than solid lines in the figures (see figures 15–18, 20, and 22). It is clear from the way they plot versus depth (compared with the thermocouple and Fe-Ti oxide data) that such glasses do not follow changes in ambient temperatures, the reason being that their MgO and CaO contents are too low to shift significantly. Thus, these glasses were metastable *prior to drilling*, and only persisted in the core because of sluggish nucleation of alkali feldspar and the SiO_2 phase (probably cristobalite).
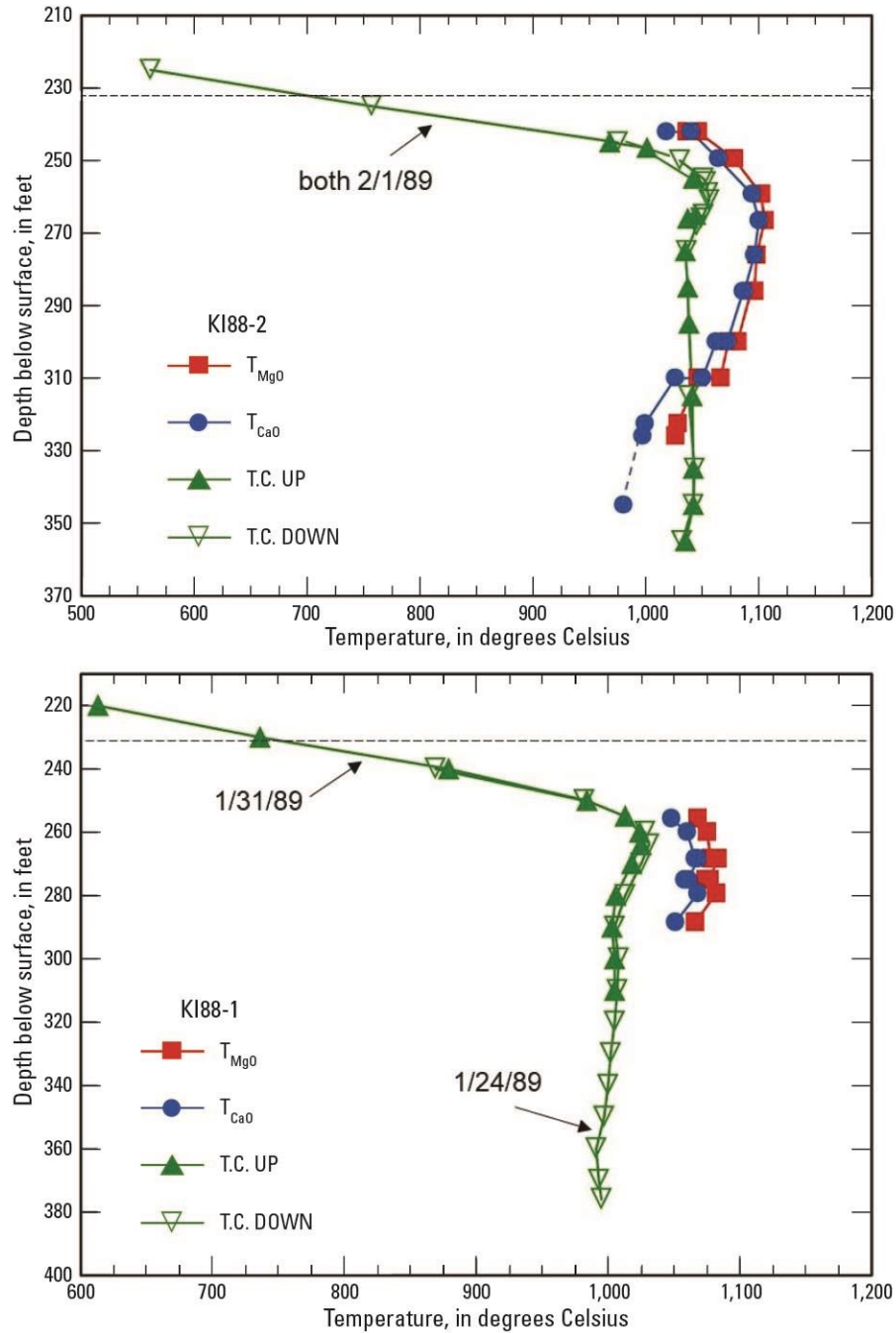
Figure 22. Graphs showing temperature variation with depth below the surface of Kīlauea Iki lava lake in the 1988 boreholes, both of which passed through the partially molten core of the lake and into subsolidus core beneath. The horizontal dashed lines indicate the depth at which hackly radial fractures were first observed in these drill cores. Dashed line for deepest KI88-2 sample indicates that the rhyolitic residual glass is metastable. Data are from appendix tables 1.1 and 2.4. See text for discussion.

The presence of such metastable glass has influenced the appearance of the drill core in the high subsolidus region. Where this glass is present, the core exhibits a hackly radial fracture on all internal broken surfaces. The first appearance of these fractures is well defined in the 1979–1988 drill cores and is indicated in figures 17–22 by a horizontal dashed line. The position of that line coincides fairly well with the upper limit of the occurrence of metastable rhyolitic glass, in those cores where both types of data are available. [In earlier cores, the onset of this fracturing is not well determined, due to gaps in recovery, abrasion of the core, and the presence of segregation veins (in which such fracturing does not develop). Also, though such fractures are present in lower-crust core from boreholes KI79-5 and KI88-1, the onset of these fractures is harder to define, perhaps because temperature varies slowly with depth in that part of the lava lake.] The data are consistent with the proposal (advanced in Helz, 1993) that these fractures form in response to shrinkage of the glass phase when hit by the water used during drilling.

Acknowledgments

References Cited

Albee, A.L., and Ray, L., 1970, Correction factors for electron probe microanalysis of silicates, oxides, carbonates, phosphates, and sulfates: Analytical Chemistry, v. 42, no. 12, p. 1408–1414. [Also available at https://doi.org/10.1021/ac60294a030.]

Anderson, A.T., and Wright, T.L., 1972, Phenocrysts and glass inclusions and their bearing on oxidation and mixing of basaltic magmas, Kīlauea Volcano, Hawaii: American Mineralogist, v. 57, no. 1–2, p. 188–216.

Barth, G.A., Kleinrock, M.C., and Helz, R.T., 1994, The magma body at Kīlauea Iki lava lake: Potential insights into mid-ocean ridge magma chambers: Journal of Geophysical Research, Solid Earth, v. 99, no. B4, p. 7199–7217.
[Also available at https://doi.org/10.1029/93JB02804.]

Bence, A.E., and Albee, A.L., 1968, Empirical correction factors for the electron microanalysis of silicates and oxides: Journal of Geology, v. 76, no. 4, p. 382–403. [Also available at https://www.jstor.org/stable/30064650.]

Buddington, A.F., and Lindsley, D.H., 1964, Iron-titanium oxide minerals and synthetic equivalents: Journal of Petrology, v. 5, no. 2, p. 310–357. [Also available at https://doi.org/10.1093/petrology/5.2.310.]

Byerly, G.R., Melson, W.G., Nelen, J.A., and Jarosewich, E., 1977, Abyssal basaltic glasses as indicators of magma compositions: Smithsonian Contributions to the Earth Sciences, no. 19, p. 22–30.

Colp, J.L., 1979, FY79 lava lake drilling program—geoscience studies; plans and results: Albuquerque, N.M., Sandia National Laboratories [report] SAND79-1361, 106 p.

Greaney, A.T., Rudnick, R.L., Helz, R.T., Gaschnig, R.M., Piccoli, P.M., and Ash, R.D., 2017, The behavior of chalcophile elements during magmatic differentiation as observed in Kīlauea Iki lava lake, Hawaii: Geochimica et Cosmochimica Acta, v. 210, p. 71–96. [Also available at https://doi.org/10.1016/j.gca.2017.04.033.]

Hardee, H.C., 1980, Solidification in Kīlauea Iki lava lake: Journal of Volcanology and Geothermal Research, v. 7, no. 3–4, p. 211–223. [Also available at https://doi.org/10.1016/0377-0273(80)90030-X.]

Hardee, H.C., Dunn, J.C., Hills, R.G., and Ward, R.W., 1981, Probing the melt zone of Kīlauea Iki lava lake, Kīlauea Volcano, Hawaii: Geophysical Research Letters, v. 8, no. 12, p. 1211–1214. [Also available at https://doi.org/10.1029/GL008i012p01211.]

Helz, R.T., 1987a, Diverse olivine types in lavas of the 1959 eruption of Kīlauea Volcano, and their bearing on eruption dynamics, *in* Decker, R.W., Wright, T.L., and Stauffer, P.H., eds., Volcanism in Hawaii: U.S. Geological Survey Professional Paper 1350, v. 1, p. 691–722. [Also available at https://doi.org/10.3133/pp1350.]

Helz, R.T., 1987b, Differentiation behavior of Kīlauea Iki lava lake, Kīlauea Volcano, Hawaii; an overview of past and current work, *in* Mysen, B.O., ed., Magmatic processes; physicochemical principles: Geochemical Society Special Publication no. 1 (a volume in honor of Hatten S. Yoder, Jr.), p. 241–258.

Helz, R.T., 1993, Drilling report and core logs for the 1988 drilling of Kīlauea Iki lava lake, Kīlauea Volcano, Hawaii, with summary descriptions of the occurrence of foundered crust and fractures in the drill core: U.S. Geological Survey Open-File Report 93–15, 57 p. [Also available at https://doi.org/10.3133/ofr9315.]

Helz, R.T., 2009, Processes active in mafic magma chambers; the example of Kīlauea Iki lava lake, Hawaii: Lithos, v. 3, no. 1–2, p. 37–46, with electronic supplement. [Also available at https://doi.org/10.1016/j.lithos.2008.11.007.]

Helz, R.T., 2012, Trace element analyses of core samples from the 1967–1988 drillings of Kīlauea Iki lava lake, Hawaii: U.S. Geological Survey Open-File Report 2012–1050, 46 p. [Also available at https://doi.org/10.3133/ofr20121050.]

Helz, R.T., and Hearn, B.C., Jr., 1998, Compositions of glasses from the Pu'u O'o-Kupaianaha eruption of Kīlauea Volcano, Hawaii, January 1983 through December 1994: U.S. Geological Survey Open-File Report 98–511, 75 p. [Also available at https://doi.org/10.3133/ofr98511.]

Helz, R.T., and Taggart, J.E., Jr., 2010, Whole-rock analyses of core samples from the 1988 drilling of Kīlauea Iki lava lake, Hawaii: U.S. Geological Survey Open-File Report 2010–1093, 47 p. [Also available at https://doi.org/10.3133/ofr20101093.]

Helz, R.T., and Thornber, C.R., 1987, Geothermometry of Kīlauea Iki lava lake, Hawaii: Bulletin of Volcanology, v. 49, no. 5, p. 651–668. [Also available at https://doi.org/10.1007/BF01080357.]

Helz, R.T., and Wright, T.L., 1983, Drilling report and core logs for the 1981 drilling of Kīlauea Iki lava lake (Kīlauea Volcano, Hawaii), with comparative notes on earlier (1967–1979) drilling experiences: U.S. Geological Survey Open-File Report 83–326, 66 p. [Also available at https://doi.org/10.3133/ofr83326.]

Helz, R.T., and Wright, T.L., 1992, Differentiation and magma mixing on Kīlauea's east rift zone; a further look at the eruptions of 1955 and 1960; part I, the later 1955 lavas: Bulletin of Volcanology, v. 54, no. 5, p. 361–384. [Also available at https://doi.org/10.1007/BF00312319.]

Helz, R.T., Banks, N.G., Casadevall, T.J., Fiske, R.S., and Moore, R.B., 1984, A catalogue of drill core recovered from Kīlauea Iki lava lake from 1967 to 1979: U.S. Geological Survey Open-File Report 84–484, 72 p. [Also available at https://doi.org/10.3133/ofr84484.]

Helz, R.T., Banks, N.G., Heliker, C., Neal, C.A., and Wolfe, E.W., 1995, Comparative geothermometry of recent Hawaiian eruptions: Journal of Geophysical Research, Solid Earth, v. 100, no. B9, p. 17,637–17,657.
[Also available at https://doi.org/10.1029/95JB01309.]

Helz, R.T., Clague, D.A., Mastin, L.G., and Rose, T.R., 2014b, Electron microprobe analyses of glasses from Kīlauea tephra units, Kīlauea Volcano, Hawaii: U.S. Geological Survey Open-File Report 2014–1090, 24 p., plus 2 appendixes in separate files. [Also available at https://doi.org/10.3133/ofr20141090.]

Helz, R.T., Clague, D.A., Sisson, T.W., and Thornber, C.R., 2014a, Petrologic insights into basaltic volcanism at historically active Hawaiian volcanoes, *in* Poland, M.P., Takahashi, T.J., and Landowski, C.M., eds., Characteristics of Hawaiian volcanoes:
U.S. Geological Survey Professional Paper 1801, chap. 6, p. 237–292. [Also available at https://doi.org/10.3133/pp1801.]

Helz, R.T., Cottrell, E., Brounce, M.N., and Kelley, K.A., 2017, Olivine-melt relationships and syneruptive redox variations in the 1959 eruption of Kīlauea Volcano as revealed by XANES: Journal of Volcanology and Geothermal Research, v. 333–334, p. 1–14.
[Also available at https://doi.org/10.1016/j.jvolgeores.2016.12.006.]

Helz, R.T., Kirschenbaum, H., Marinenko, J.W., and Qian, R., 1994, Whole-rock analyses of core samples from the 1967, 1975, 1979 and 1981 drillings of Kīlauea Iki lava lake, Hawaii: U.S. Geological Survey Open-File Report 94–684, 65 p.
[Also available at https://doi.org/10.3133/ofr94684.]

Jarosewich, E., Nelen, J.A., and Norberg, J.A., 1979, Electron microprobe reference samples for mineral analysis: Smithsonian Contributions to the Earth Sciences, no. 22, p. 68–72.

Murata, K.J., and Richter, D.H., 1966, Chemistry of the lavas of the 1959–60 eruption of Kīlauea Volcano, Hawaii: U.S. Geological Survey Professional Paper 537–A, 26 p. [Also available at https://doi.org/10.3133/pp537A.]

Pallon, J.E., Okamura, R.T., Sako, M.K., and Wright, T.L., 1994, A summary of leveling data from Kīlauea Iki lava lake from 1960 to 1988: U.S. Geological Survey Open-File Report 94–137, 33 p. [Also available at https://doi.org/10.3133/ofr94137.]

Pitcher, L., Helz, R.T., Walker, R.J., and Piccoli, P., 2009, Fractionation of the platinum-group elements and Re during crystallization of basalt in Kīlauea Iki lava lake, Hawaii: Chemical Geology, v. 260, no. 3–4, p. 196–210. [Also available at https://doi.org/10.1016/j.chemgeo.2008.12.022.]

Rae, A.S.P., Edmonds, M., Maclennan, J., Morgan, D., Houghton, B., Hartley, M.E., and Sides, I., 2016, Time scales of magma transport and mixing at Kīlauea Volcano, Hawaii: Geology, v. 44, no. 6, p. 463–466. [Also available at https://doi.org/10.1130/G37800.1.]

Richter, D.H., and Moore, J.G., 1966, Petrology of the Kīlauea Iki lava lake, Hawaii:
U.S. Geological Survey Professional Paper 537–B, 26 p. [Also available at https://doi.org/10.3133/pp537B.]

Richter, D.H., Eaton, J.P., Murata, K.J., Ault, W.U., and Krivoy, H.L., 1970, Chronological narrative of the 1959–60 eruption of Kīlauea Volcano, Hawaii: U.S. Geological Survey Professional Paper 537–E, 73 p. [Also available at https://doi.org/10.3133/pp537E.]

Scowen, P.A.H., Roeder, P.L., and Helz, R.T., 1991, Re-equilibration of chromite within Kīlauea Iki lava lake, Hawaii: Contributions to Mineralogy and Petrology, v. 107, no. 1, p. 8–20. [Also available at https://doi.org/10.1007/BF00311181.]

Sio, C.K.I., Dauphas, N., Teng, F.-Z., Chaussidon, M., Helz, R.T., and Roskosz, M., 2013, Discerning crystal growth from diffusion profiles in zoned olivine by in-situ Mg-Fe isotopic analyses: Geochimica et Cosmochimica Acta, v. 123, p. 302–321. [Also available at https://doi.org/10.1016/j.gca.2013.06.008.]

Stovall, W.K., Houghton, B.F., Hammer, J.E., Fagents, S.A., and Swanson, D.A., 2012, Vesiculation of high fountaining Hawaiian eruptions; episodes 15 and 16 of 1959 Kīlauea Iki: Bulletin of Volcanology, v. 74, no. 2, p. 441–455. [Also available at https://dx.doi.org/10.1007/s00445-011-0531-7.]

Teng, F.-Z., Dauphas, N., Helz, R.T., Gao, S., and Huang, S., 2011, Diffusion-driven magnesium and iron isotope fractionation in Hawaiian olivine: Earth and Planetary Science Letters, v. 308, no. 3–4, p. 317–324. [Also available at https://doi.org/10.1016/j.epsl.2011.06.003.]

Wright, T.L., and Okamura, R.T., 1977, Cooling and crystallization of tholeiitic basalt, 1965 Makaopuhi lava lake, Hawaii: U.S. Geological Survey Professional Paper 1004, 78 p. [Also available at https://doi.org/10.3133/pp1004.]